Organisms use mode-switching to solve the explore-vs-exploit problem

Debojyoti Biswas[1], Andrew Lamperski[2], Yu Yang[3], Kathleen Hoffman[4], John Guckenheimer[5], Eric S. Fortune[6], and Noah J. Cowan[1,3,*]

[1]Laboratory for Computational Sensing and Robotics, Johns Hopkins University, Baltimore, MD, USA.
[2]Department of Electrical and Computer Engineering, University of Minnesota, Minneapolis, MN, USA.
[3]Department of Mechanical Engineering, Johns Hopkins University, Baltimore, MD, USA.
[4]Department of Mathematics and Statistics, University of Maryland, Baltimore County, Baltimore, MD, USA.
[5]Department of Mathematics, Cornell University, Ithaca, NY, USA.
[6]Federated Department of Biological Sciences, New Jersey Institute of Technology, Newark, NJ, USA.
[*]e-mail: ncowan@jhu.edu

Abstract

The inescapable link between sensing and movement in organisms generates a behavioral conflict between producing costly movements for gathering information ("explore")[1–3] versus using previously acquired information to achieve a goal ("exploit").[4] Determining the optimal balance between explore and exploit is a computationally intractable problem,[5–7] necessitating the use of heuristics to understand how organisms resolve this conflict.[8] Here we show that the electric fish *Eigenmannia virescens*[2,3,9] uses a mode-switching strategy to solve the explore–exploit conflict[8] during a refuge tracking task,[10–13] and this strategy is modulated by sensory salience. The fish produced distinctive non-Gaussian (i.e., non-normal) distributions of movement velocities characterized by sharp peaks for slower, task-oriented "exploit" movements and broad shoulders for faster, "explore" movements. Surprisingly, the measures of non-normality increased (rather than decreased) in relation to increased sensory salience. Reanalysis of published data for additional ten species revealed that phylogenetically diverse organisms, from amoebae to humans[14–22] : (i) produce this distinctive distribution of movement velocities, and (ii) exhibit the same counter-intuitive modulation of mode-switching in relation to sensory salience. We propose a parsimonious, state-uncertainty based mode-switching heuristic that reproduces the distinctive velocity distribution, and explains its relationship to sensory salience. This mode-switching strategy likely manifests in diverse biological mechanisms, from cellular processes for single-cell motility to network-level processes for the control of movement in organisms.

Main

Organisms display complex patterns of movement that arise from the interplay between obtaining information ("explore") and using current information ("exploit"). Exploratory movements to gain information, and exploitative movements to achieve the task at hand, are often mediated by the same motor systems. For example, the weakly electric glass knifefish (*Eigenmannia virescens*) produces both information-seeking exploratory movements[2,3,9] and goal-driven exploitative movements to remain within the refuge[10,13] using the same ribbon-fin locomotor system.[23,24] Both of these types of movement occur in a single linear dimension, along the rostrocaudal axis. This behavior makes *E. virescens* an excellent model system with which to investigate the interplay between explore and exploit movements: within a fixed refuge, fish produce ancillary back and forth exploratory movements to sense the refuge,[2,3,9] but these back and forth movements conflict with the exploit goal of station keeping.

Resolving this conflict between explore movements[9] versus goal-directed exploit movements is a computationally intractable optimization problem.[5–7] How do organisms resolve the explore–exploit conflict? A simple heuristic to solve this problem would be for an organism to perform goal-directed exploit movements while superimposing continuous small exploratory sensing movements—in other words to use a persistent excitation approach.[25] Indeed, this heuristic has proven effective (if suboptimal) as an engineering approach to solve the explore–exploit problem of identifying states and parameters of a dynamical system during task execution.[25] If organisms were to employ such a strategy, they would produce movement statistics that correspond to a single behavioral mode (e.g., a single component Gaussian distribution) that continuously superimposes explore and exploit behavior.

However, we discovered that *E. virescens* does not use a persistent excitation strategy; instead, it exhibits a mode-switching strategy between fast (explore) and slow (exploit) behavioral modes. This mode switching is modulated by sensory salience in a counter-intuitive manner (Fig. 1–2). To assess the generality of this mode-switching strategy we investigated additional ten tasks performed by ten species ranging from amoebae to humans,[14–22] using five major sensing modalities–vision, audition, olfaction, tactile sensing and electrosensation (Fig. 3). Based on this extensive reanalysis we found that such mode switching—and its counter-intuitive dependence on sensory salience—is found across diverse behaviors, taxa, and sensing modalities (Fig. 4).

Inspired by this widespread biological solution to the explore–exploit problem, we propose an engineering heuristic for selecting modes based on state uncertainty (Fig. 5) that captures the key structural features of mode switching found across organismal models. The mode-switching heuristic achieves similar task-level performance but with less control effort than that of the persistent excitation strategy.

E. virescens exhibited fast and slow behavioral modes

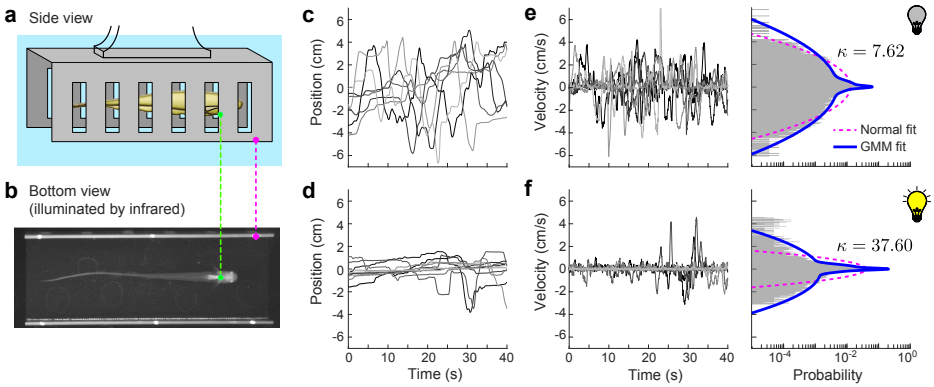

Fig. 1. Velocity distributions are broad-shouldered. (a) Side view (schematic) and (b) bottom view (infrared image) of a fish inside a stationary refuge. The bright ventral patch on the fish was tracked (green dot) as the fish swam inside the refuge (magenta dot). (c,d) Position traces during (c) lights-off trials ($n = 7$), and (d) lights-on trials ($n = 10$) from a single representative fish. (e,f) Corresponding velocity traces during lights-off trials (left) and velocity histogram (right) over the same range of velocities for (e) lights-off, and (f) lights-on trials, with the kurtosis value κ indicated; note that the time and probability scales of the horizontal axes are shown below panel (f). A three-component Gaussian mixture model (GMM; blue solid curve) fit the data better than the normal fit (magenta dashed curve) as indicated by the lower Kullback-Leibler divergence and Bayesian information criterion values; see Extended Data Table 1 for statistical details. One lights-off trial with large positive velocity is truncated; see Extended Data Fig. 1a,b for full version.

We examined the behavior of individual *E. virescens* as they performed untrained station keeping within a fixed refuge. Station keeping requires only small corrective movements; therefore any significant movements by the fish are attributed to information-seeking, exploratory movement.[2,3,9] Previous work[12] has demonstrated that *E. virescens* use both vision and electrosense for station-keeping. Hence varying light level is an experimental mechanism to examine the effect of visual salience on the selection between explore and exploit movements.

We measured the movements of five individual fish in 40 s duration station-keeping trials, in two lighting conditions: lights "on" trials had bright illumination (∼80 lx), and lights "off" trials had low illumination (∼0.3 lx). We conducted between 7 and 10 trials per condition per fish. The order of lights-on and lights-off trials were randomized.

We discarded trials in which the fish changed its swimming direction or exited the refuge. Consistent with prior studies,[2,9] fish moved significantly more in lights-off conditions than in lights-on conditions (Extended Data Fig. 1).

The patterns of fish swimming velocities were consistent with a mode-switching strategy. The distribution of velocities (v) featured a sharp peak around $v = 0$ with "broad" shoulders for faster movements (Fig. 1e,f, right). These empirical distributions differed from a Gaussian distribution in two ways: (i) the distinct central peak, and (ii) the broad shoulders corresponding to the faster movements. The central peak (near zero velocity) represents slow movement, and the broad shoulders represent faster movement. These behavioral modes are associated with exploit and explore respectively, as discussed in greater detail below.

The two behavioral modes were significantly better approximated by three-component Gaussian mixture models (GMMs) than by single component models (Fig. 1e,f, right). This was shown by three measures, namely Kullback-Leibler (K-L) divergence, Bayesian information criterion (BIC), and closeness of quantile-quantile (Q-Q) plots to the reference line (Extended Data Table 1, Extended Data Fig. 2). The three component GMMs generally comprised a sharp central Gaussian peak, capturing slow, task-oriented station-keeping movements, and two Gaussian "shoulders", capturing faster, positive (forward) and negative (backward) exploratory movements. We found that only modest improvements in the fit of the GMMs occurred when using more than three components (Extended Data Fig. 1f).

The fast mode movements increased in frequency in lights-off trials, increasing the relative prominence of the "shoulders". For example, Fig. 1e,f show representative data from one fish in which there were 48 fast movements with lights off (Fig. 1e, left) but only 13 fast movements with lights on (Fig. 1f, left). Interestingly, the overall higher proportion of fast velocities in lights-off trials leads to a surprising result, namely higher kurtosis values for lights-on versus lights-off trials (Extended Data Fig. 1e). In other words, the increase in frequency of fast motions in the dark leads to a decrease in the relative prominence of the central, task-oriented velocity peak at $v = 0$, so that the overall distribution is closer to Gaussian, and the kurtosis trends toward 3.

We found that the trend towards a Gaussian distribution of movement velocities in lights-off trials (reduced sensory salience) to be surprising because the exploratory movements for actively sensing the environment are associated with a nonlinear requirement[26,27] to make movements that are potentially in conflict with task goals. Therefore, our initial hypothesis– that this nonlinearity would produce *increased* deviation from a Gaussian velocity distribution as sensory salience was *reduced*–was not supported. Our initial intuition failed because we did not appreciate that decreases in sensory salience drives the selection of explore behavior, and that behavior itself is approximately Gaussian, ultimately reducing the relative prominence of the task-oriented central peak.

Interestingly, reanalysis of data from a previous study of exploratory movements in a similar refuge tracking paradigm in *E. virescens* show the same relationship between sensory salience and changes in velocity profiles, but for modulations of a different sensory modality, namely electrosensation.[3] In these previous experiments, artificially generated electrical signals were used to diminish the salience of electrosensory information as the electric fish performed the refuge tracking. Our reanalysis of these published data (see Supplementary Material and Methods for details) showed that fish exhibited the distinctive non-Gaussian distribution of velocities. Moreover, the velocity distributions were modulated in relation to electrosensory salience: lower kurtosis values (corresponding to more normal distributions) occurred in experimental trials with added artificial electrosensory "jamming" signals (Extended Data Fig. 3).

Sensory salience drives explore–exploit mode switching

How do changes in sensory salience drive changes in mode switching? To investigate this question, we segregated the velocity trajectories into "S", a slow velocity mode (exploit) comprising task-oriented, station-keeping movements, and "F", a fast velocity mode (explore) comprising large positive (forward) and negative (backward) movement velocities (Fig. 2a,b, Extended Data Fig. 4) (see Methods for segregation clustering algorithm).

Fish produced slow and fast velocity modes of movements in both lights-on and lights-off trials. We computed the residence time in each behavioral mode as a proportion of the total time spent in that mode compared to the trial duration of 40 s (note that the residence time in slow and fast modes adds up to unity). The residence time τ_s in the slow exploit mode was significantly higher (> 1.7 times) in lights-on trials than the lights-off trials (Fig. 2c). In contrast, the residence time in the fast explore mode ($1 - \tau_s$) was higher in light-off than in lights-on trials.

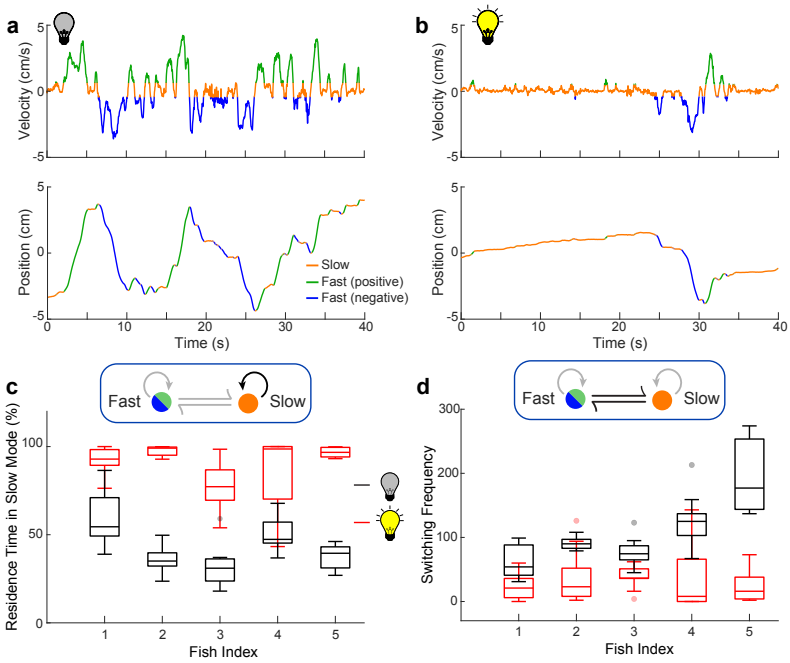

Fig. 2. Bursts of faster movements are more common in lights-off trials than in lights-on trials. (a,b) Fish showed two distinct behavioral modes, slow movement and fast movement, as seen in the velocity (top) and position traces (bottom) of representative trials from the same fish under lights-off (a) and lights-on (b) conditions. (c) The residence time in the slow mode, computed as the percent of the trial duration (40 s), was significantly higher during lights-on trials than lights-off trials (one sided p-value < 0.002 for each fish). (d) The switching between the fast mode (positive and negative combined) and slow mode was significantly more frequent in lights-off trials (black) than in lights-on trials (red) (one-tailed p-value < 0.002 for each fish). For both (c,d), the p-values were calculated using the Mann-Whitney-Wilcoxon test.

Fish switched between slow and fast modes more frequently in lights-off trials than in lights-on trials (Fig. 2d). From the computation of the transition rates between slow (S) and fast (F) modes as a two-state Markov process, we found that the transition rate S $\rightarrow$ F was significantly lower in lights-on versus lights-off trials, i.e., the slow (exploit) state was visited more frequently in the lights-on trials compared to lights-off trials (Extended Data Fig. 5). This salience-dependent modulation of switching frequency was the key mechanism by which movement velocity distributions trended toward a Gaussian distribution as a function of decreased sensory salience.

Mode-switching is found across taxa, behaviors, and sensory modalities

Is this mode-switching strategy solution for the explore versus exploit problem found in other species, in other categories of behavioral tasks, and in control systems that rely on other sensing modalities?

To answer this question we analyzed published data for additional ten species, representing a wide phylogenetic range of taxa, from single-celled organisms to humans, involving categorically different tasks and sensorimotor regimes.[3,14–20,22] These taxonomically diverse species were selected to encompass a wide range of behaviors that rely on a broad range of sensory systems (Fig. 3). For every example we examined, we found the same distinctive non-normal distribution of velocities, with a peak at low velocity movements and broad shoulders for higher velocity movements (Fig. 4).

For example, postural sway movements in humans are thought to prevent the fading of postural state information during balance.[28] Our reanalysis of quiescent stance data[17] revealed evidence of mode switching (Fig. 4a) that is remarkably similar to our findings in electric fish. In the quiescent stance task, human subjects used visual and tactile feedback to maintain an upright posture. The distribution of sway velocities revealed a distinct peak at low velocities corresponding to the task goal, and broad shoulders for higher velocities produced by the exploratory movements; the velocity statistics were better captured by a GMM than a normal distribution. Furthermore, the velocity distribution showed the same surprising relation to changes in salience, (becoming more Gaussian when

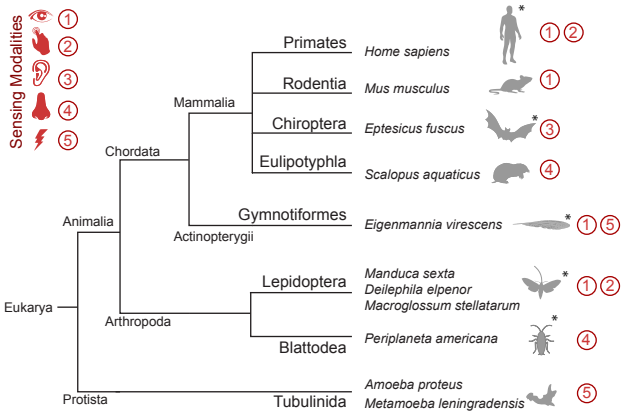

Fig. 3. Diversity of organisms and sensing modalities used for analysing mode-switching strategies. The major sensing modalities (vision, tactile sensing, audition, olfaction, and eletrosensation) used for task execution are listed next to the organisms (four species of mammals, a species of ray-finned fish, four species of insects, and two species of amoebae). The effect of sensory salience is studied for organisms marked with asterisks. Behaviors and movement statistics of the organisms are shown in greater detail in Fig. 4.

sensory salience was decreased (Extended Data Fig. 6), as seen in the electric fish *E. virescens*.

Mode switching was also observed in invertebrate species. For example, the Carolina sphinx hawkmoth (*Manduca sexta*) uses somatosensory feedback from their proboscis to detect the curvature of flowers when searching for nectaries at dawn and dusk.[20] In this search behavior, which has dynamics that are qualitatively similar to vibrissal sensing in rats,[29] the moth sweeps its proboscis across the surface of the flower using a combination of slow- and high-velocity movements. Our analysis of the distribution of the rate of change of radial orientation angle (angle between the proboscis tip trajectory and the radial axis of the flower), before the insertion of the proboscis tip into the nectary shows the characteristic sharp peak with broad-shoulders (Fig. 4g) that is captured by a GMM. Experimental changes in the shape of artificial flowers that degrade the salience of the curvature of the flower surface[20] resulted in a decrease of the kurtosis value of the proboscis angular velocity distribution (Extended Data Fig. 12), similar to how both *E. virescens* and humans responded to changes in sensory salience.

The fact that this salience-based, mode switching strategy was found in two distantly related classes (mammalia and insecta) performing very different behaviors, using different sensorimotor systems, suggests that the strategy emerged as a convergent solution to the explore versus exploit problem. We found additional evidence of convergence of this solution in reanalysis of eight additional datasets: visual saccades in humans (Fig. 4b, Extended Data Fig. 7)[21] and in house mice *Mus musculus* (Fig. 4c, Extended Data Fig. 8),[15] movements of the pinnae of echolocating big brown bats *Eptesicus fuscus* (Fig. 4d, Extended Data Fig. 9),[16] olfaction in Eastern moles *Scalopus aquaticus* (Fig. 4e, Extended Data Fig. 10)[14] and American cockroaches *Periplaneta americana* (Fig. 4f, Extended Data Fig. 11),[18] and visual tracking of a swaying flower in three species of hawkmoths (*Manduca sexta, Deilephila elpenor, Macroglossum stellatarum*) (Fig. 4h, Extended Data Fig. 13).[19] The discovery of a similar, parsimonious velocity distributions across taxa, behavior, and sensing modalities, with consistent dependency on sensory salience, was surprising.

Intriguingly, our analysis of the dynamics of transverse exploration by pseudopods of amoebae[22] (*Amoeba proteus* and *Metamoeba leningradensis*) reveals similar GMM velocity distributions in response to an electric field (Extended Data Fig. 14). Although our modeling approach (see next section) includes inertial dynamics, that cannot be directly applied to movement of organisms in the low Reynolds number regimes occupied by single-celled and other microscopic organisms, these observations are consistent with a mode-switching strategy for the control of movement in these amoebae.

The examples described above include a broad phylogenetic array of organisms that perform a variety of behavioral tasks using different control and morphophysiological systems. Just as these behavioral systems evolved within each of the lineages represented in our reanalyses, we suggest that mode switching likely evolved independently in each system as well. In other words, the similarities we found across taxa are the result of convergent evolution towards a common solution—mode switching—for the explore versus exploit problem.

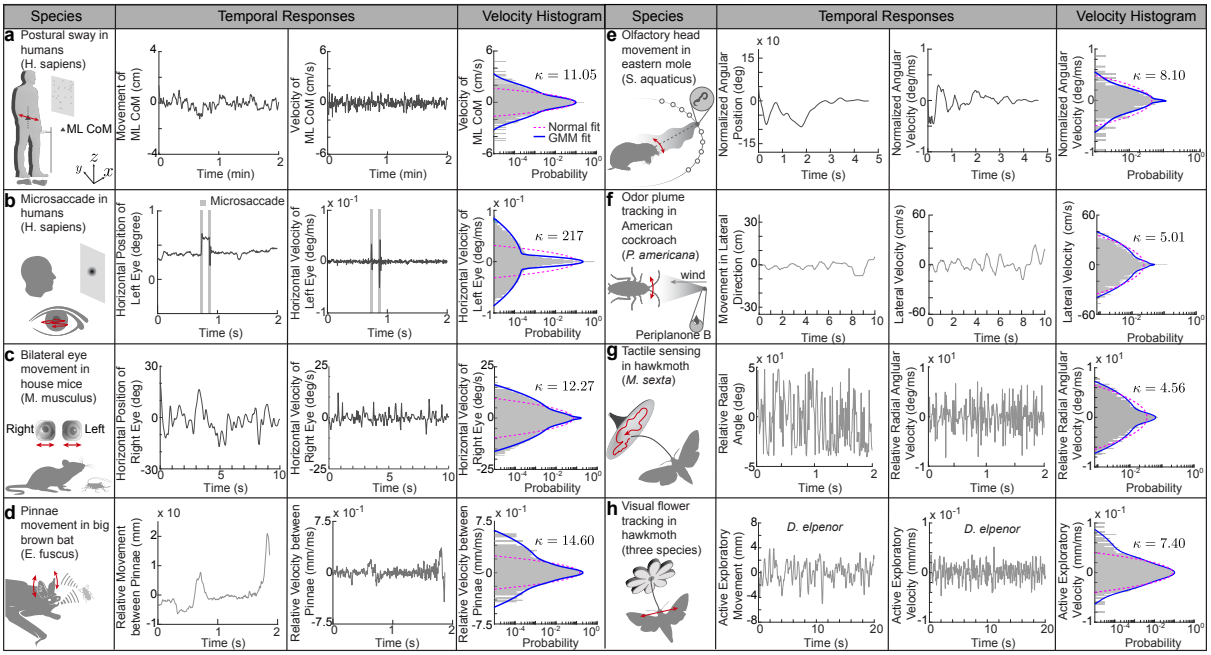

Fig. 4. Mode switching is a robust feature across taxa, behaviors, and sensing modalities. Reanalysis of data from eight prior studies reveals a convergent statistical structure of movements across a range of organisms and behaviors: (a) postural sway in humans (*Homo sapiens*) during maintenance of quiet upright stance,[17] (b) microsaccades in humans (*Homo sapiens*) during fixated gaze,[21] (c) bilateral eye movements in mice (*Mus musculus*) during prey (cricket) capture,[15] (d) pinnae movements in big brown bats (*Eptesicus fuscus*) while echolocating prey (mealworm),[16] (e) olfactory driven head movements in eastern moles (*Scalopus aquaticus*) in response to food (earthworms),[14] (f) odor plume tracking in American cockroaches (*Periplaneta americana*) in response to sex pheromone (Periplanone B),[18] (g) tactile sensing by Carolina sphinx hawkmoth (*Manduca sexta*) while searching for a flower nectary,[20] and (h) visual tracking of swaying flower by hawkmoths[19] (three species; only data from elephant hawkmoth, *Deilephila elpenor* is shown, for the remainder see Extended Data Fig. 14).The second column shows representative temporal traces of the active exploratory movements, the third column shows the respective velocity traces. The fourth column presents velocity histograms showing that, unlike the normal distribution (magenta dashed curve), the three- component Gaussian mixture model (GMM; blue solid curve) captures the broad-shouldered nature of the velocity data across species, behaviors, and sensing modalities. See Extended Data Table 2 for statistical details. Photo credit: Mice eye image courtesy of authors in Michaiel *et al.*,[15] published under the terms of the Creative Commons Attribution License.

Heuristic Model of the Explore–Exploit Mode-Switching Strategy

Why might animals use mode switching, rather than the simpler heuristic of applying continual, low-amplitude exploratory inputs used by adaptive control engineers[25]?

To address this question, we propose a parsimonious heuristic model that comprises a nonlinear motion-dependent sensor, a linear musculoskeletal plant, a state estimator, and a mode-switching controller (Fig. 5a). The key feature of the model is that the nonlinear sensory system embodies the high-pass filtering (i.e., fading or adapting) characteristics found across biological sensory systems.[30–32] This sensory system model ("motion dependent sensor" in Fig. 5a) assumes nonlinear measurements that decay to zero over time in the face of constant stimuli. Previous theoretical work has demonstrated that exploratory movements are required for state estimation in control systems that rely on such high pass (i.e., fading) sensors.[26,27] All details of the modeling can be found in the Methods.

The controller includes a state-feedback-based task level control policy, $-f(\hat{x}, \hat{v})$, that exploits previously collected sensory information; that information is parsimoniously encoded in (i) estimates of the position and velocity $(\hat{x}, \hat{v})$, and (ii) in an ongoing measure of uncertainty (a function of the covariance of position and velocity estimates), M_ε. The controller also includes an active sensing control policy, $u_a(t)$, that seeks to gain new information through exploratory movements. We tested three exploratory movement heuristics for the controller:

1. **Zero Excitation:** This is a passive strategy (i.e., no exploration) in which the system provides no input excitation for the actuation forces ($u_a(t) = 0$ for all t). This is a conventional state-feedback controller.

2. **Persistent Excitation:** This scheme tests a common continuous exploration strategy used in the field of adaptive control.[25] The controller continually injects a Gaussian input $u_a(t)$.

3. **Triggered Excitation:** This mode-switching strategy depends on lower and upper thresholds, $T_{\min}$ and $T_{\max}$; the controller only injects Gaussian input when the uncertainty in the state estimator M_ε exceeds $T_{\max}$, and then continues to inject input until this uncertainty drops below a lower threshold, $T_{\min}$ (Extended Data Fig. 15a).

As prior theoretical work shows,[27] the Zero Excitation strategy (i.e., traditional state-estimate feedback) cannot minimize the state estimation error (e_{RMS}, Fig. 5b, left), thus illustrating the need for an additional active sensing component in the face of adaptive sensing and perceptual fading.

The Persistent Excitation and Triggered Excitation strategies both facilitate substantially better position control than does the Zero Excitation strategy (Fig. 5b, middle and right). Though these two strategies resulted in comparable state-estimation errors (e_{RMS}, Fig. 5b, middle and right), the Triggered Excitation was more efficient, requiring substantially lower control effort (u_{RMS}, Fig. 5c, middle and right). Moreover, unlike the Persistent Excitation strategy, Triggered Excitation generated a distinctive broad-shouldered velocity distribution that featured a sharp peak near zero, with broad shoulders corresponding to bursts of fast movement (Fig. 5d, middle and right). This distribution was strikingly similar to experimental observations across organisms (Fig. 1 and Fig. 4).

The choice of thresholds in the Triggered Excitation strategy plays an important role in shaping the velocity to best extract sensory information, in a way that reduces control effort; with low thresholds, the statistics approach that of the Persistent Excitation, whereas high thresholds lead to velocity distributions with higher kurtosis (departure from normality), while requiring less control effort (Extended Data Fig. 15b–d).

How does sensory salience affect performance of the Triggered Excitation (mode-switching) heuristic? To simulate the effects of changes in sensory salience, we parametrically varied the sensory noise variance while keeping constant the switching thresholds $T_{\min}$ and $T_{\max}$. As the sensory noise variance was increased (simulating a decrease in salience), the kurtosis value of the velocity distribution decreased, numerically approaching normality in the limit of high sensory noise (Extended Data Fig. 16).

This trend of decreased kurtosis in the face of increased noise variance captures the widespread observation that in animals the velocity statistics tend toward a Gaussian distribution as sensory salience is decreased. Moreover, the underlying mechanism, namely increasing frequency of bursts of exploratory movements, matches our experimental observations in *E. virescens*, which performed more frequent transitions to fast movements and spent less time in the slow mode in the lights-off trials than in the lights-on trials (Fig. 2c,d). These analyses clarify that this trend toward a Gaussian distribution with decreased salience is an epiphenomenon of mode-switching: as the frequency of fast movement bursts increases, it overwhelms the task-oriented movements, diminishing the prominence of the central peak.

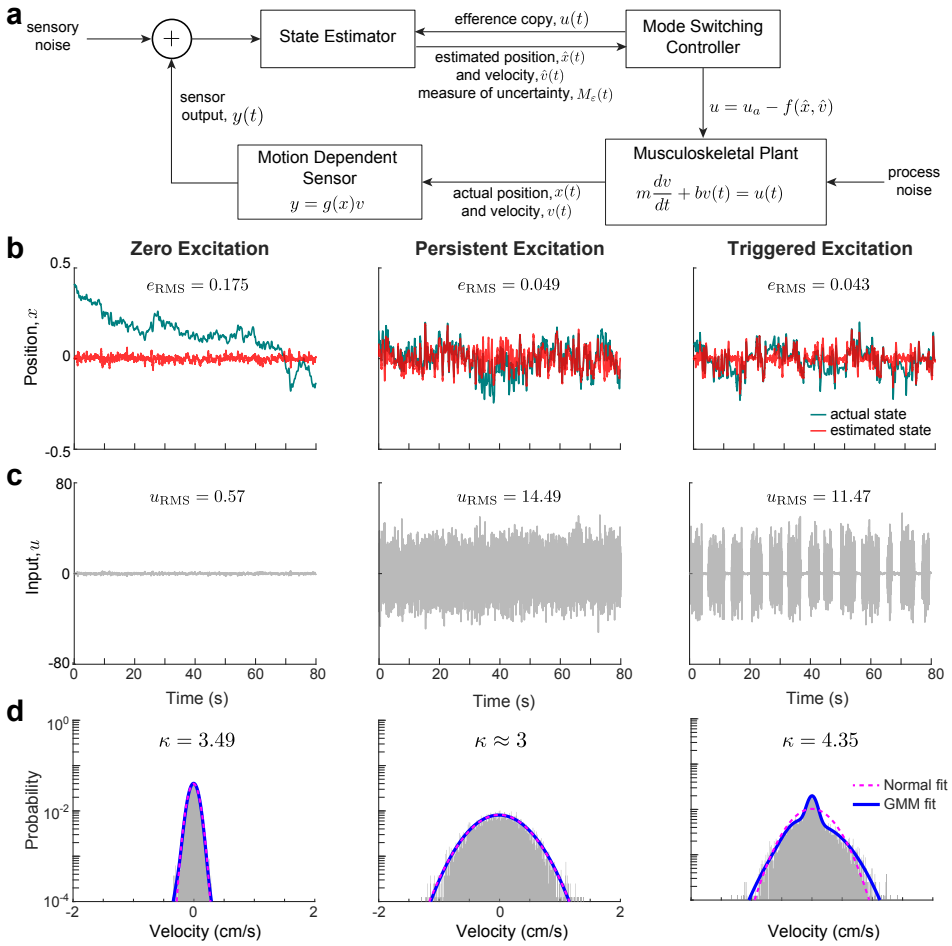

Fig. 5. Template model illustrating three different exploration strategies. (a) Schematic of a mode-switching strategy. The musculoskeletal plant for animal locomotion has two states—position (x) and velocity (v). The state estimator has access to noisy measurements from a nonlinear adaptive sensor ($g(x)v$). The state estimator (extended Kalman filter) is designed to work in tandem with the mode switching controller. The controller output, u comprises both state-feedback ($-f(\hat{x}, \hat{v})$) and an active control component ($u_a(t)$). See Methods for details. (b) Simulated position traces (actual states: teal, estimated states: red) using three different exploratory movement strategies for $u_a(t)$: Zero Excitation (left), Persistent Excitation, i.e., continuous Gaussian (middle), and Triggered Excitation (right) along with the state- feedback. Although both Persistent and Triggered Excitation inject Gaussian input, only the Triggered Excitation strategy injects the Gaussian signal when the measure of uncertainty (M_ε) reaches a threshold (see Methods). The respective RMS values of the state estimation error (e_{RMS}) are shown in the panels. (c,d) Controller input traces (c) and velocity histograms (d) for various schemes as in (b). Respective RMS values of the inputs (u_{RMS}) are shown in the panels of (c). Note that the Triggered Excitation scheme achieves comparable positional estimation error despite substantially lower input energy. In (d) the fits with a normal distribution (magenta dashed) and three-component Gaussian mixture model (blue solid) are shown along with the respective kurtosis (κ) values.

Discussion

We examined explore-exploit tradeoffs in the context of goal-direct motor behaviors, such as station keeping, postural balance, and plume tracking, that require active, exploratory movements to enhance sensation. Similar tradeoffs have been extensively studied in categorically different domains, including foraging[32,33] and reinforcement learning.[34] Here we show that the velocity distributions that emerge from the interplay between exploratory movements and goal-directed control are broad-shouldered across taxa, and that this distinctive distribution of movements is robustly modulated by sensory salience. The bouts of ancillary movements that comprise the broad shoulders of these velocity distributions are commonly described as "active sensing", i.e., the expenditure of energy by organisms for the purpose of sensing[35,a]. Active sensing research in humans, in relation to touch, was popularized in sixties by J.J. Gibson,[1] and the original ideas date back at least to the 18th century (for a historical account, see Zweifel *et al.*[35]).

Surprisingly, active sensing is largely avoided in engineering design despite being ubiquitous in animals. The performance of engineered systems may benefit from the generation of movement for improved sensing. An algorithm known as Ergodic Information Harvesting (EIH)[3] could be used to control movements for sensing in artificial systems. This algorithm balances the energetic costs of generating movements against the expected reduction in sensory entropy. The EIH has been tested in relation to several animal model systems, and produces plausible animal trajectories.[3]

Interestingly, the EIH algorithm produces the opposite trend in kurtosis of velocity distributions in relation to sensory salience (Extended Data Fig. 17, Extended Data Table. 3) that we observed in our experiments, reanalysis of prior data, and in our model: as sensory salience decreases, there is an increase in active sensing movements but a decrease in kurtosis (Extended Data Table. 2). That EIH leads to decrease in kurtosis occurs in part because EIH generates continuous sensing movements, and does not incorporate mode switching. A refined EIH model, that generates the temporally distinct periods of sensing movements that characterize mode switching, would better reflect our findings in animals, and is a promising strategy for improving the performance of robotic control systems.

How mode switching is manifest across the diverse biological systems we examined is a compelling open question. Many of these control systems have evolved via convergent evolution in which adaptive strategies emerge independently across lineages. One result of convergent adaptation is that species often rely on idiosyncratic features, such as feathers or skin flaps, to achieve the same adaptive strategy, such as flapping flight. We infer that the mechanisms for mode switching is present in control systems that range from sub-cellular systems[41] to neural systems in vertebrates.

The mechanisms for mode switching in vertebrate nervous systems may emerge at different levels within sensorimotor control pathways. For example, neurophysiological recordings show that sensory salience can be encoded in brain circuits via synchronization and desynchronization of spiking activity.[42] Such population coding of salience,[43–45] when coupled with a threshold, could trigger discrete bursts of motor activity for sensing.[23] Motor circuits for the production of discrete bursts of movement occur in spinal circuits.[46]

These discrete bursts of movements could arise from reflex-like, threshold-based activity in animals, akin to how Mauthner cells trigger a cascade of motor activity when sensory inputs exceed a threshold.[47] A key difference between reflex-like, threshold-based behaviors and the mode-switching we describe in this paper would be that the signal in question would arise from an internal representation of sensory uncertainty, rather than from the overall level of sensory excitation. Such a reflex-like action could produce stereotyped forms of interactions with the external environment in relation to sensing.[23]

Environmental noise makes it difficult for organisms to gather sufficient sensory information without making large exploratory movements. However, increased exploration would lead to increased energy expenditure, time to task completion, and even predation risk. We contend that occasional (as contrasted with continuous) exploratory movements stimulated by internal representations of uncertainty could enable organisms to safely meet sensory demands on a limited energy budget. Our simplified heuristic model provides a first step at rationalizing this hypothesis. Notwithstanding the limitations of this simplified theory, the ubiquity of mode switching itself, and its specific and strong dependence on sensory salience, is clear.

[a] Active sensing includes not only the sorts of ancillary movements described here, but also the emission of energetically costly signals such as electric fields by weakly electric fishes[36] and echolocation calls in dolphins, birds, and bats.[37–40] The emission and reception of these electrical and acoustic signals are also affected by movements of the individual, which has been a focus of our work in electric fishes.[2,9,23]

Methods

Tracking of glass knifefish

Subjects

We obtained adult, weakly electric, glass knifefish *Eigenmannia virescens* (10 – 15 cm in length) from commercial vendors, and housed the fish according to the published guidelines.[48] Water temperature in the experimental tank was kept between 24 – 27 °C, and conductivity ranged from 10 – 150 µS/cm. Fishes were transferred from the holding tank to the experimental tank 12 – 24 hours prior to the experiments, to allow for acclimation. All experimental procedures were approved by the Johns Hopkins Animal Care and Use Committee, and followed guidelines established by the National Research Council and the Society for Neuroscience.

Experimental apparatus

The experimental apparatus was similar to that used in previous studies.[2,10–12,23] The refuge was machined from a 152 mm long segment of 46 × 50 mm rectangular PVC tubing, with the bottom surface removed to allow the camera to record the ventral view of the fish. On both sides of the refuge, a series of six rectangular windows (6 mm wide × 31 mm high, spaced 19 mm apart) were machined, through which to provide visual and electrosensory cues.

A computer sent designed digitized input stimuli (25 Hz) from LabView (National Instruments, Austin, TX, USA) to a FPGA based controller for a stepper motor (STS-0620-R, HW W Technologies, Inc., Valencia, CA, USA). The stepper motor drove a linear actuator, leading to the one degree of freedom refuge movement in real time. A video camera (pco.1200, PCO AG, Kelheim, Germany) captured fish movements through mirror reflection at 100 Hz. The captured frames (width × height: 1280 pixels × 276 pixels) were saved as 16 bits .tif files via camera application software (pco.camware, PCO AG, Kelheim, Germany).

Experimental procedure

The experiments were conducted in two illuminance levels—around 0.3 lx (lights off) and 80 lx (lights on). Each trial lasted for 60 s. During the initial 10 s of each trial, the refuge was actuated to follow a 0.45 Hz sinusoidal trajectory, the amplitude of which was gradually increased to 3 cm, and then decreased to 0 at the end of the 10 s interval, in a similar fashion as described in Biswas *et al.*[2] After the initiation phase, the refuge remained stationary for 40 s, finally followed by a termination phase for 10 s, during which the refuge was actuated in a similar fashion as during the initiation phase.

Tracking Algorithm

To observe fine details of the fish movement, we used a high frame rate in our video recordings. High tracking accuracy was essential as the position and velocity data were likely to be contaminated by measurement noise. To ensure high tracking accuracy, the refuge and fish position were analyzed by custom video tracking software[49] developed by Balázs P. Vágvölgyi from the Laboratory for Computational Sensing and Robotics (LCSR), at Johns Hopkins University.

The tracking algorithm worked in two phases. The first phase was template matching, which roughly located the targets (fish or refuge). In the first frame of a given video, a rectangular region was manually selected around the target to create a template. On subsequent frames, a neighborhood region around the template (± 20 pixels) from the previous frame was selected for the computation of a normalized 2-D cross-correlation matrix. If the target changed its orientation in the new frames, before computing the normalized 2-D cross-correlation, the new image frame was first rotated to match the orientation of the template from previous frame. If needed, the areas of the image were sampled (then scaled and interpolated if necessary) with subpixel accuracy.

After creating the template, the second phase applied the Levenberg-Marquardt algorithm to find the global maximum of the normalized cross-correlation function. This step produced a match between the template and target at each frame, with subpixel accuracy. We performed extensive preliminary testing and analysis to confirm that the remaining measurement errors had smaller variance than the stochastic movements of the fish.

Data Processing

The tracking algorithm stored the fish position in both horizontal and vertical directions, (originally in pixels, along with the respective pixel to meter conversion factor), and the angle of orientation (in degree) in .csv files. We used only the data while the refuge was stationary (40 s, 4000 data points in total) for each trial. To further reduce the measurement noise, the position data was filtered through a Butterworth zero-phase distortion filter (`filtfilt` command in MATLAB) with a 15 Hz cutoff frequency. Fish velocity in the horizontal direction was computed as forward differences of the horizontal position time series.

Identification of Behavioral Modes

For the identification of the behavioral modes, the velocity data from each individual fish at a specific lighting condition were clustered into three components, slow, fast positive, and fast negative, using two velocity thresholds, v_L and v_H ($v_L < v_H$), resulting in two behavioral modes—slow and fast (fast positive and negative were combined).

These threshold values were computed by finding the inflection points of the fitted Gaussian mixture model (GMM), f_{GMM}, to the respective velocity data specific to a lighting condition. To numerically identify the inflection points of f_{GMM}, we located the first and the last indices of the array $\frac{f''_{\text{GMM}}}{f_{\text{GMM}}}$ such that the condition $\frac{f''_{\text{GMM}}}{f_{\text{GMM}}} < c$ was satisfied for a given c. This method separated the central peak of the f_{GMM}, velocity distribution around zero velocity, from the broad shoulders. We chose $c = 0.005$ for all the individual fish irrespective of the lighting conditions, except for fish 1 lights-off trials ($c = 0.02$), (the different x-value for fish 1 lights-off trials was chosen so that the relative area under the central peak of the distribution was less than 0.6 (similar to other fish during lights-off trials).

Simulation

For the musculoskeletal plant, we assumed a simplified second-order Newtonian model:[26]

$$\begin{aligned} \frac{dx(t)}{dt} &= v(t), \\ \frac{dv(t)}{dt} &= -\frac{b}{m}v(t) + \frac{1}{m}u(t) + w_1(t). \end{aligned} \tag{1}$$

Here $x(t)$ is dimensionless position, $v(t)$ is dimensionless velocity, $u(t)$ is the controller input, and $w_1(t)$ is process noise. The process noise includes noise due to physical disturbances[50,51] as well as motor noise.[52] The system parameters m and b represent unitless mass and viscous damping, respectively.

For the "motion dependent sensor", we assumed a nonlinear measurement model[26,27] with sensory noise $w_2(t)$:

$$y(t) = \frac{d}{dt}s(x(t)) + w_2(t) = g(x)v(t) + w_2(t). \tag{2}$$

Here, $s(x)$ is the position dependent sensory scene experienced by the organism. For the present study, we assumed a quadratic sensory scene $s(x) = \frac{1}{2}\alpha x^2 + \beta x$ with nonzero constant sensory scene parameters α and β. This assumption on sensory scene yields $g(x) = \alpha x + \beta$, a linear function of position, x. Due to the presence of the nonlinearity in the measurement, we assumed an extended Kalman filter (EKF) as the state estimator. The mode-switching controller includes a traditional state-estimate-feedback component, $-f(\hat{x}, \hat{v})$, with estimated position and velocity, $(\hat{x}, \hat{v})$, as well as an active control component, $u_a(t)$. For the state-feedback component we assumed $f(\hat{x}, \hat{v}) = k_1\hat{x} + k_2\hat{v}$. In the Triggered Excitation scheme, for the uncertainty measure (M_ε) we used the trace of the state estimation error covariance matrix, $\text{Tr}(P(t))$. When the uncertainty measure $M_\varepsilon(t)$ rose above a maximum threshold, $T_{\max}$, the controller generated $u_a(t)$ as a Gaussian input with fixed power spectral density and it continued to inject the input until $M_\varepsilon(t)$ dropped below a lower threshold, $T_{\min}$. At this point the controller switched back to traditional state-feedback form. For the Persistent Excitation scheme, the controller continued to inject a Gaussian input $u_a(t)$ for all time. The systems parameters were chosen from:[10,26] $b = 1.7$, $m = 1$, $\alpha = 3$, $\beta = 5$, $k_1 = m\omega_n^2$, $k_2 = (2m\zeta\omega_n + b)$, $\zeta = 0.56$, $\omega_n = 1.05 \times 2\pi$, $T_{\max} = 0.006$, $T_{\min} = 0.005$. The process noise, $w_1(t)$ and sensor noise, $w_2(t)$ were assumed to be Gaussian noise inputs with variance 0.03 and 10, respectively. Both Persistent and Triggered Excitation injected Gaussian white noise of variance 20.

Statistics

All the statistical analysis was performed with Mann-Whitney-Wilcoxon (MWW) test using custom codes written in MATLAB (Mathworks, Natick, MA, USA). For all tests, the significance level was set to 0.05. The experimental and simulation data are provided as either mean plus or minus the standard deviation ($\mu\pm$SD) or mean plus or minus the standard error of the mean ($\mu\pm$SEM).

Data and software availability

Before final submission, an archived version of the datasets and the analysis code supporting this article will be made available through the Johns Hopkins University Data Archive.

Acknowledgement

We thank Tim Kiemel (UMD) for providing human balance data and Balázs P. Vágvölgyi (JHU) for developing the tracking software used in this work. We thank Cynthia F. Moss (JHU), Varun P. Sharma (GT) and Simon Sponberg (GT) for suggesting relevant articles for the reanalysis of the animal locomotion data, and Sarah L. Poynton (JHMI) for critical feedback on the manuscript. This work was supported by Office of Naval Research under grant no. N00014-21-1-2431 (N.J.C).

Author contribution

Conceptualization, all authors; Methodology, all authors; Software, D.B., A.L., K.H., Y.Y. and J.G.; Formal Analysis, D.B., A.L., K.H., Y.Y. and J.G.; Investigation, Y.Y.; Data Curation, D.B. and Y.Y.; Writing – Original Draft, all authors; Writing – Review and Editing, all authors; Visualization, D.B. with other authors; Supervision, N.J.C.

Declaration of Interests

The authors declare no competing interests.

Supplementary Materials and Methods

All experimental data for reanalysis were acquired from prior studies either directly through the authors[17] or published dataset.[14–16,18–20,22] All computations for reanalysis were performed using custom MATLAB scripts.

Refuge tracking of glass knifefish in presence of jamming electrodes

We examined experimental data for refuge tracking of *E. virescens* under varying electrosensory conditions from a prior study.[3] In that study, a rectangular refuge was actuated to follow a sinusoidal trajectory of frequency 0.1 Hz and amplitude of 17 mm (in contrast to the stationary refuge in our study). The fish position was tracked at 60 Hz. The experiments were conducted in the dark, in the presence of a closed-loop jamming system, where the frequency of the jamming signals was set to 5 Hz below the electric organ discharge (EOD) frequency of the fish.

To extract the active exploratory movements from the refuge tracking response, we first computed the Fourier transform of the original temporal response of fish, deleted the frequency peak corresponding to the refuge motion (0.1 Hz) from the frequency response, and then reconstructed the time domain signal using an inverse Fourier transform. To estimate the velocity of the active exploratory component, we scaled the forward difference of position data.

Postural sway in humans

The experimental data of human postural sway in the upright stance were acquired from a prior study[17] through the authors. In the original experiment, nine healthy adults (subjects) maintained a modified tandem Romberg stance for 4 min. The trials were performed under four different multi-sensory conditions, with different combinations of vision and tactile sensing: (i) neither vision nor touch, (ii) only vision, (iii) only touch, and (iv) both vision and touch.

In the present study, we analyzed the data for conditions ii, iii, and iv in which the subjects use vision and/or tactile cues. Data for the mediolateral center of mass (ML CoM) were collected from a sensor attached to each subject's lower back (at the level of the fourth or fifth lumbar vertebra). We excluded the data from two subjects as they were too noisy, thus we used $N = 7$. The original data were collected at a frame rate of 50 Hz. We subsampled the data at 5 Hz to reduce the noise in the velocity data, which was computed from forward differences.

Saccadic eye movements in humans

The data for eye movements in humans during fixated gaze at a stationary object, were acquired from a prior study involving five adult humans (subjects) with normal or corrected-to-normal vision.[21] The subjects were instructed to look at circular stimuli of different levels of Gaussian blur, and matched summed intensities on the screen, at a distance of 175 cm. The eye movements of the subjects were recorded using an Eyelink 1000 eye tracker. The original data were collected at 1000 Hz, then smoothed by the previous authors using a third-order Savitzky-Golay filter of frame length 21 ms. The prior authors also removed blink periods, as well as the data 200 msbefore and 300 ms after each blink.

In the velocity data we detected and removed outliers (velocity value greater than 1.5×10^{-5} degree/ms) degree/ms) that were likely caused by measurement errors; these outliers comprised only 0.05% of the original data.

Bilateral eye movements in house mice

Data for eye movements in freely moving house mice, *Mus musculus*, during capture of prey (crickets) in a closed arena, were acquired from a prior study.[15] Eye tracking and head movement were classified by the original authors into two different behavioral phases (Extended Data Fig. 8a,b): (i) approach and (ii) non-approach. During the approach phase, the head of the mouse was oriented towards the cricket (the azimuthal angle was within $\pm 45^o$), and was moving faster than 1cm/s. During this approach phase, the left and right eye movements were more synchronized with each other than in the non-approach phase, in which the eye movements were erratic and often moved in the opposite direction to each other.

In our present study, we focused on the data during the non-approach phases, as the abrupt saccades were not directly related to the tracking of the prey to facilitate its capture. We assumed the exploratory eye movements during the non-approach phase were largely driven by the need for sensing. The approach phase behaviors were short ($\approx 5.8\%$ of the whole dataset), whereas non-approach segments were long and more frequent. The original dataset

had 105 trajectories collected from seven mice at a frame rate 30 Hz. The data contained some discontinuities due to tracking loss. To fill those missing data, we used the moving a median method with window length of 30 samples. The eye velocity data was computed from forward differences.

Pinnae movements in big brown bats

The echolocation data were acquired from a prior study[16] of the pinnae movement in big brown bats, *Eptesicus fuscus*, in relation to the prey trajectories. The prey target were mealworms, tethered to a wire, which were moved from an initial distance of 2.5 m toward the bats, trained to rest on a platform. For our current analysis, we considered two of the four conditions originally presented:[16] (i) single-target simple-trajectory (Extended Data Fig. 9b left), and (ii) single-target complex-trajectory (Extended Data Fig. 9b right). In the former scenario, there was only forward movement of the target toward the bats; in the latter case the target was was receded twice before finally arriving at the bat platform. The dataset had 10 trajectories for each condition, collected from three bats at frame rate 500 Hz. The echolocation calls of the bats were classified into "approach" and "buzz" phases.[53] The approach phase was characterized by the relatively constant and higher pulse duration and pulse interval, whereas the buzz phase was characterized by a sharp drop in both. A distance threshold of 0.5 m between the mealworms and the bats roughly correlated with the onset of the buzz phase (Fig. 1B,C in[16]).

We focused on examining the data during the approach phase only. From the z-positions of the tip of the pinnae, we computed the relative pinnae movement, Z_{L-R} as the difference between z-positions of left and right pinnae tips. From this we then computed the rate of change of this relative movement using forward differences in Z_{L-R}.

Analysis of odor tracking in Eastern moles

Blind Eastern moles *Scalopus aquaticus* are known for their excellent odor tracking capability. We took the tracking data of moles locating a stationary odor source (small sections of earthworms), in a semicircular arena, from a published dataset,[3] which was digitized from the original study.[14] Among the three original experimental conditions, we only considered the case of normal airflow where the moles had their two nostrils open. The dataset comprises six trajectories from two moles. To align the data with respect to the destination, we subtracted the last from the angular position data. Although the frame rate for data collection was not stated in the original study, it was reported that the moles usually found the odor sources in $5 - 10$ s, and the longest data sequence had 125 frames. Thus, we set the frame rate at 25 frames per second when computing the angular velocity using forward differences.

Odor plume tracking in American cockroach

Plume tracking data of adult male American cockroaches, *Periplaneta americana*, were acquired from a published dataset[3] which derived from a prior study.[18] The head position was tracked in males during their tracking task of locating the source of female sex pheromone (Periplanone B) in a laminar flow tunnel (with wind speed 25 cm/s) under red and infrared light. To understand the role of the olfactory sensors on the antennae, the authors conducted experiments in which either one antenna (unilateral) or both antennae (bilateral) were cut to specific lengths. The original data were collected at a frame rate of 30 Hz, which was later subsampled by the original authors at 15 Hz.

In the present study, we only considered lateral movement of the head for cockroaches in which there had been bilateral shortening of the antennae.

Analysis of tactile sensing in Hawkmoths

Hawkmoths (F. Sphingidae) use their proboscis to actively explore the flower surface in search of the nectary. We acquired the tactile sensing data for the Carolina sphinx hawkmoth, *Manduca sexta* from a prior study[20] through the published dataset. In the original experiment, the moths were presented with 3-D printed flowers (modeled after the corolla), with four different cross-sectional curvature profiles. We analyzed data for three profiles, "funnel", "near-funnel", and "near-flat", for the moth's first and seventh visit to the flowers. In the experiment, the tip and base of the unfurled proboscis, and the antennae were tracked at a frame rate of 100 Hz. The prior study reported two parameters: (i) normalized relative radial distance (RRD), which was computed as the distance from the proboscis tip to the center of the flower normalized to the radius of the flower; and (ii) the relative radial orientation angle (RRA) angle, which was computed as the angle between the proboscis tip trajectory and radial axis which was further wrapped to restrict the range to $0 - 90$ degree.

On successful insertion of the proboscis, the sharp decrease in the RRD indicated that the moth had started feeding from the nectary. Based on this observation, we divided each trial into two phases: pre-feeding and feeding, where the transition frame was manually selected by inspection of the data. We only used the tracking data pertinent to the pre-feeding phase. We discarded the trials where these two phases were not distinct. We computed the rate of change of RRA (ω_{RRA}) from forward differences.

Analysis of visual tracking of flower by Hawkmoths

Hawkmoths rely heavily on visual inputs to track a swaying flower, and hover during tracking, with lighting conditions affect the tracking behavior.[19] We analyzed tracking data published in an earlier study.[19] In the original experiment, three species of hawkmoths (nocturnal *Deilephila elpenor*, diurnal *Macroglossum stellatarum*, and crepuscular *Manduca sexta*) were presented with a 3-D printed flower which was actuated by a stepper motor following a sum-of-sine stimulus. The experiments were performed at three different illuminance levels: 300, 15, 0.3 lx for *D. elpenor*; 3000, 300, 15 lx for *M. stellatarum*; 300, 15, 0.3 lx for *M. sexta*. The datasets were collected at 100 Hz.

For our present analysis, we considered the data for 15 and 300 lx being the common lux levels tested across all three species of hawkmoths. To extract the active exploratory movements from the tracking response, we first computed the Fourier transform of the original temporal response, then removed the frequency peaks corresponding to the flower motion from the frequency response, and finally reconstructed the time domain signal using an inverse Fourier transform. The velocity was estimated from forward differences of position data.

Analysis of galvanotaxis in amoebae

Amoebae have served as a classic model for studying the movement of eukaryotic cells in response to various chemical, mechanical, and electrical cues. Galvanotaxis (movement in response to electric field) data of movement of two related unicellular organism *Amoeba proteus* and *Metamoeba leningradensis* were acquired from a prior study[22] through the published dataset. The experiments were performed in batches (experimental replicates). Each time a small group of amoebae was placed in a custom-made chamber with simplified Chalkley medium: *A. proteus* (experimental replicates: 8, number of cells per replicate: 4–8), *M. leningradensis* (experimental replicates: 4, number of cells per replicate: 4–15). Crowding of cells was avoided for ease in tracking individual cell as well as to eliminate any coordinated interaction among cells. Once a laminar flux was established in the experimental chamber, an electric field was applied with a gradient of 334–342 mV/mm. to study the galvanotaxis. The original data comprising trajectories of 50 cells of each species, were collected at 0.1 Hz.

In the present study we focused on the movement in the transverse direction of the applied electric field. The velocity was estimated from forward differences of position data.

Extended Data Figures

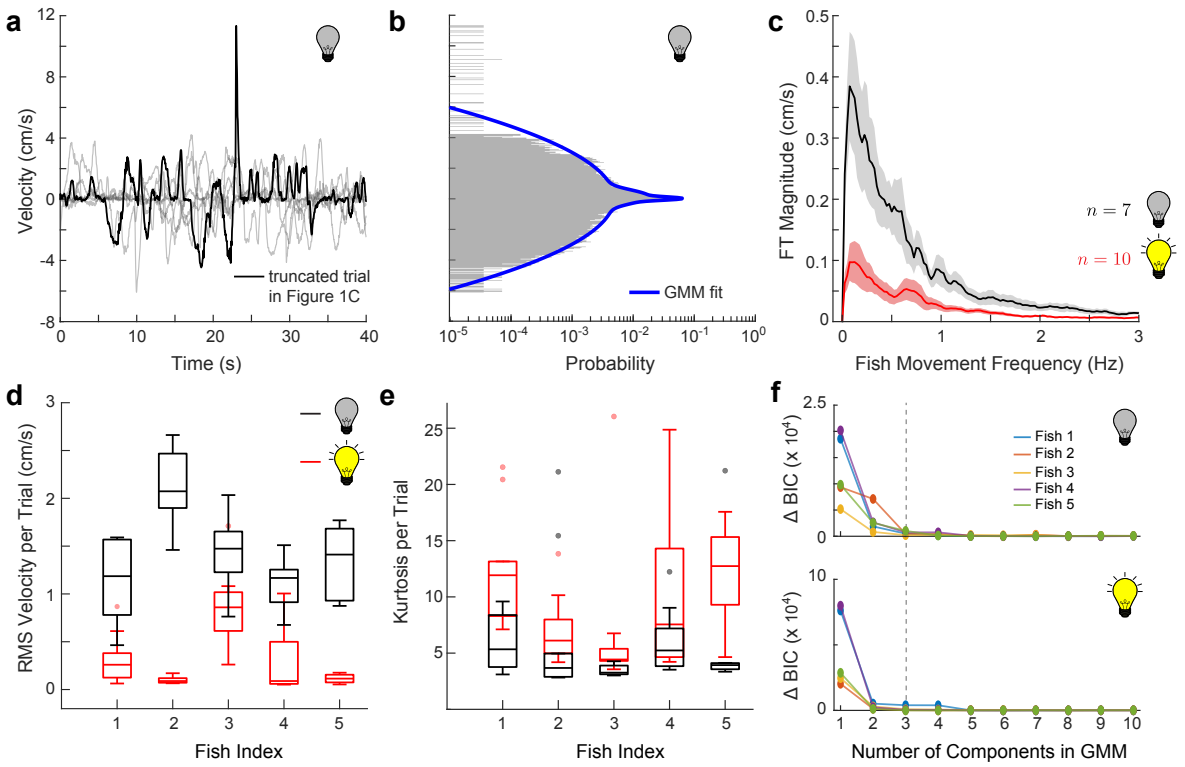

Extended Data Fig. 1. Comparison of fish movement in lights-on trials versus lights-off trials. (a) Velocity trace of the truncated trial data (black) with traces from other trials (gray) for fish 1 from Fig. 1c. (b) Histogram of all trials ($n = 7$) using same length scale, and the three-component Gaussian mixture model (GMM) fit. (c) Magnitude of Fourier transform of velocity traces with total number of trials (n) indicated next to the plots. The solid line and the shaded region denote mean and the standard error of mean, respectively. (d) Box and whisker plot showing RMS values of individual trials for all fish ($N = 5$) with colors the same as in (c). Mean RMS velocity across trials for all fish in lights-off trials was greater than in lights-on trials (one-tailed p-value < 0.005). (e) Box and whisker plot showing kurtosis values of individual trials for all fish ($N = 5$)with colors the same as in (c). For all fish, mean kurtosis values across trials in lights-on trials was greater than in lights-off trials (one-tailed p-value < 0.05). (f) Bayesian information criterion (BIC) values for varying number of components in GMM (top: lights off; bottom: lights on). The gray dashed line corresponds to three-component GMM. All p-values were calculated using the Mann-Whitney-Wilcoxon test.

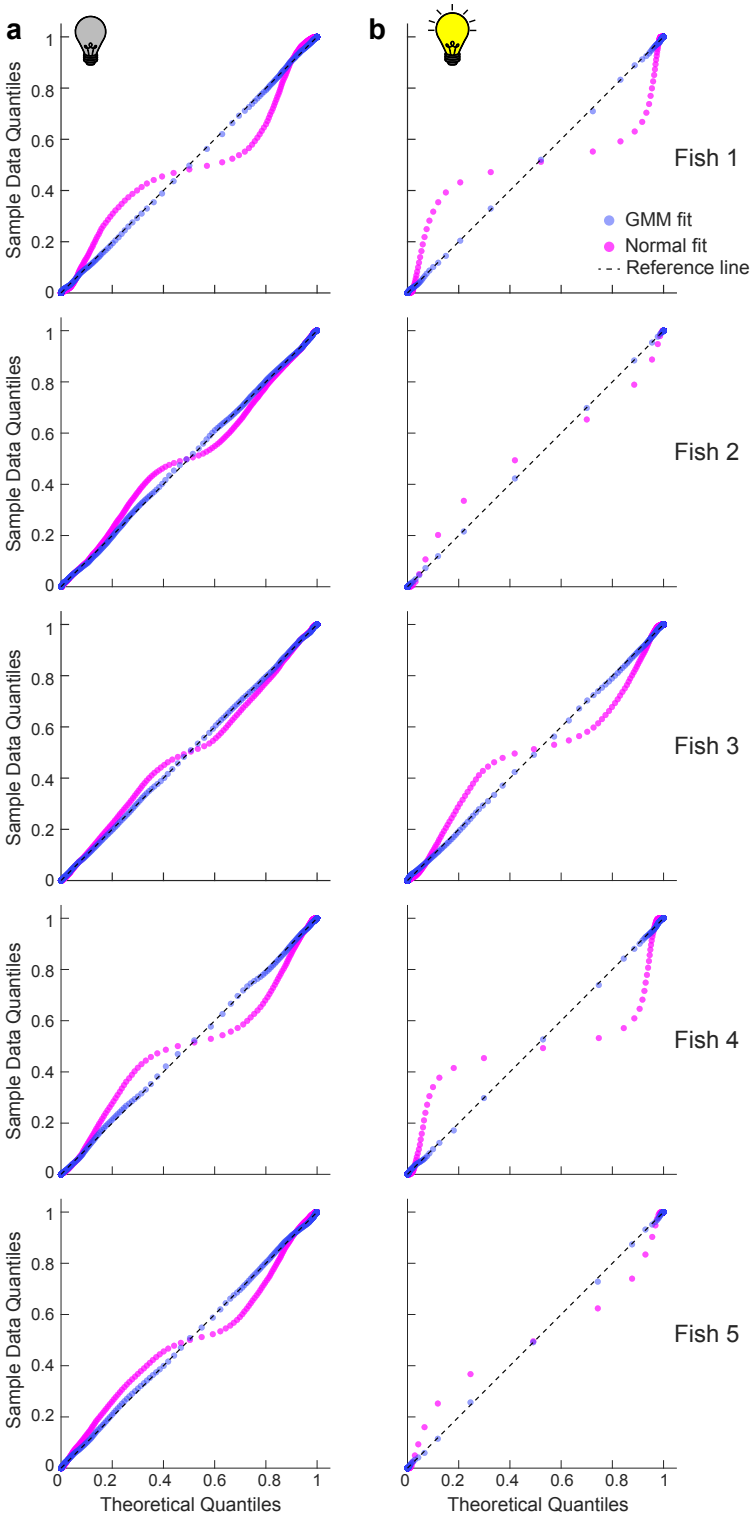

Extended Data Fig. 2. Q-Q plots of velocity traces are consistent with mode-switching. a, b) Q-Q plots comparing the velocity data for each fish ($N = 5$) from lights-off (a) and lights-on trials (b) with theoretical quantiles from a normal fit (magenta) and GMM fit (blue), respectively. Lesser deviation from the reference line (black dashed) for GMM fits with three components than for the normal, suggested better fitting of the former. The Q-Q plots also showed that the lights-off trial data were closer to normal distribution fits than were those of lights-on trial data.

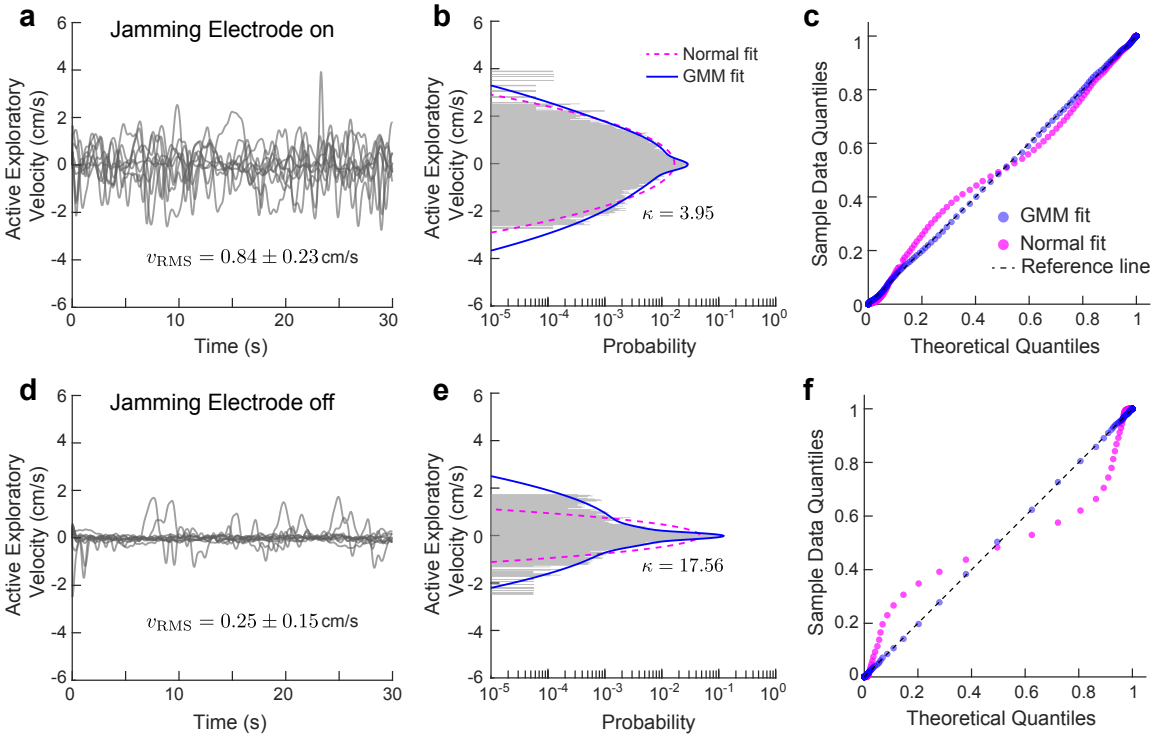

Extended Data Fig. 3. Analysis of the experimental data from *Eigenmannia virescens*[3] with jamming electrodes reveals similar non-normal trends in the velocity distributions. (a) Velocity traces ($n = 10$) with electrical "jamming" of the fish electrosensory system, which decreased the salience and reliability of electrosensory navigation. (b) Corresponding histogram, with the kurtosis value, κ. The magenta dashed and the blue solid curves correspond to a normal and GMM fit with three components, respectively. (c) Q-Q plots comparing the sample velocity data for all trials ($n = 10$) from (a) with theoretical quantiles from the same normal (magenta) and GMM fit (blue) from (b). Clearly, the GMM fit was better than the normal. See Extended Data Table 2 for statistical details. (d–f) Velocity traces ($n = 10$) with jamming electrode off (d), corresponding histogram (e) with the kurtosis value, κ and the Q-Q plots (f). Colors and styles are same as in (a–c). Mean ± SD of the respective RMS values of velocity (v_{RMS}) are shown next to plots of (a,d).

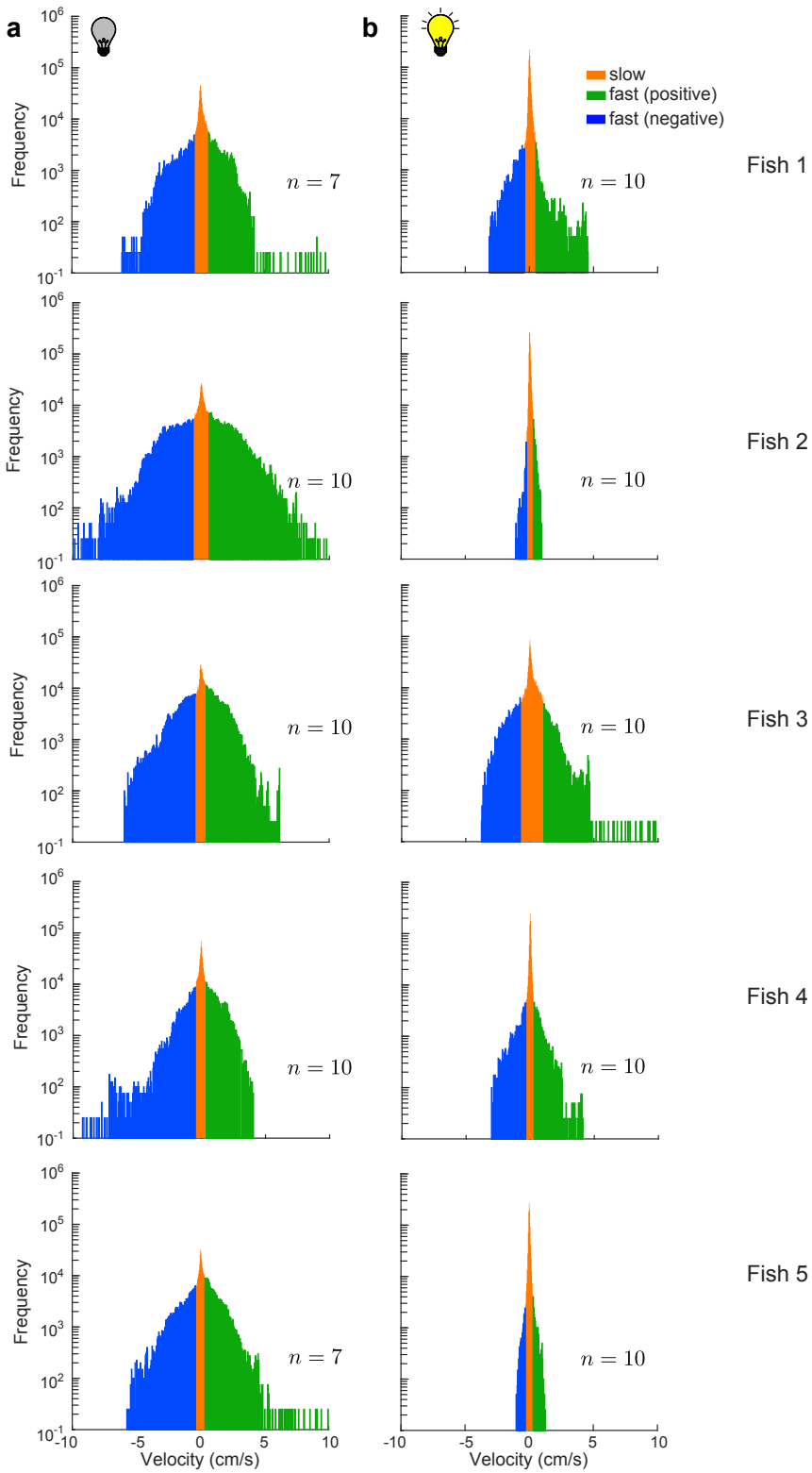

Extended Data Fig. 4. Clustering of velocity data into different behavioral modes. (a,b) Velocity histograms of lights-off (a) and lights-on (b) trials with three clusters: slow (orange), fast positive (green) and fast negative (blue). The clustering was based on a velocity threshold algorithm (see Methods for details).

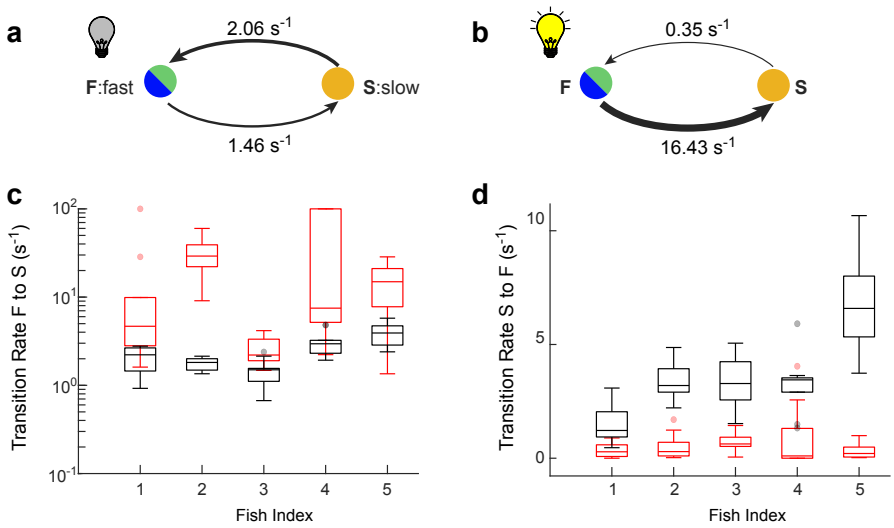

Extended Data Fig. 5. Two-state Markov model and transition rates. (a,b) Two-state (F: fast velocity both positive and negative combined and S: slow velocity) Markov process showing mean transition rates for a representative individual in lights-off (a) and lights-on trials (b). (c,d) Transition rates corresponding to state transitions: F $\rightarrow$ S in (c) and S $\rightarrow$ F in (d), respectively for lights-on (red) and lights-off (black) trials. The transition rate for F $\rightarrow$ S was higher in lights-on trials (one-tailed p-value ≤ 0.02) whereas the rate for S $\rightarrow$ F was higher in lights-off trials (one-tailed p-value < 0.003). All p-values were calculated using the Mann-Whitney-Wilcoxon test.

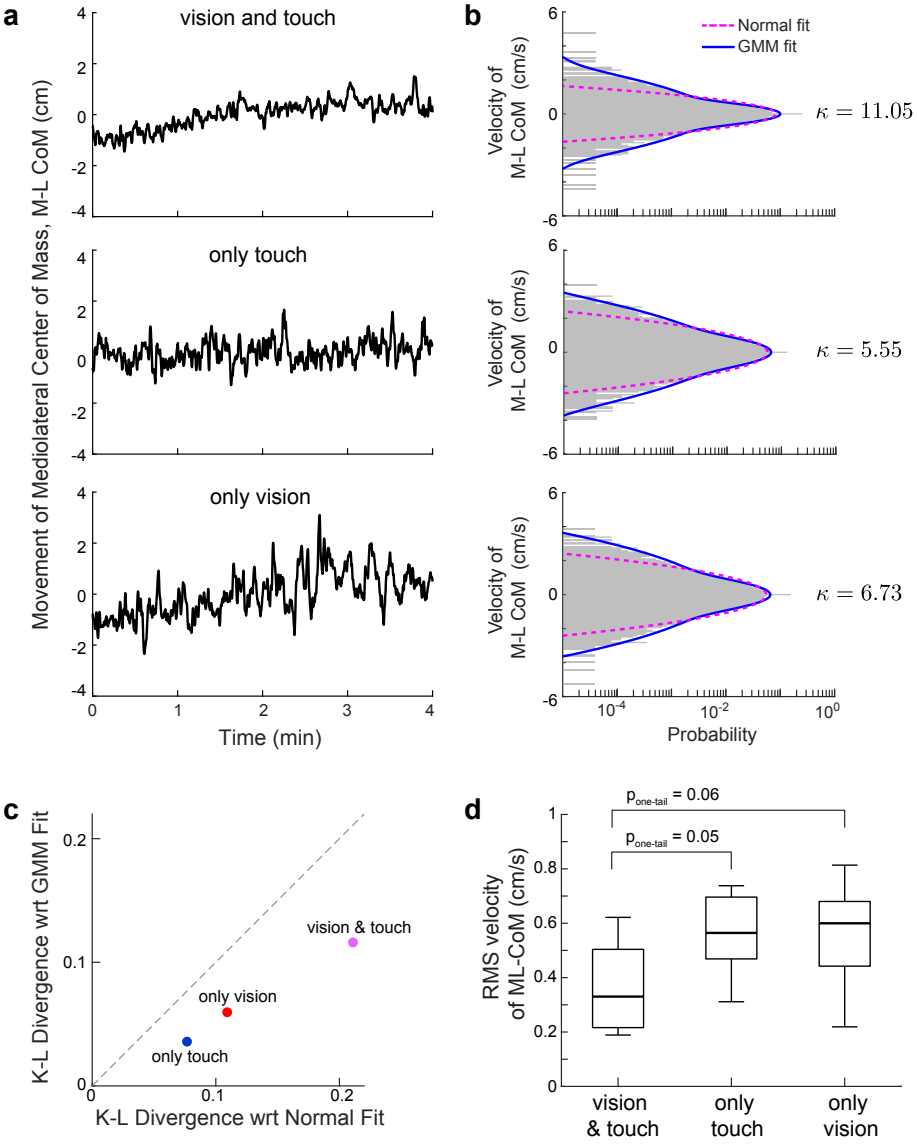

Extended Data Fig. 6. Reanalysis of the postural sway in humans, *Homo sapiens*.[17] (a,b) Representative temporal traces of mediolateral movement of center of mass, ML CoM (a) and the histograms of ML CoM velocities (b) for different experimental conditions—both vision and touch (top), only touch (middle) and only vision (bottom). The magenta dashed and the blue solid curves in (b) correspond to a normal and GMM fit with three components, respectively. The dataset analyzed here, comprised of 7 subjects, with three replicate trials per experimental condition, was collected at 50 Hz. (c) Plot of K-L divergence values for GMM fit vs Normal fit. Colors denote different experimental conditions. All the markers lying below the unity slope line indicated that the GMM better approximated the data. (d) Comparison of the RMS velocities for different experimental conditions. The one-tailed p-values were computed using the Mann-Whitney-Wilcoxon test.

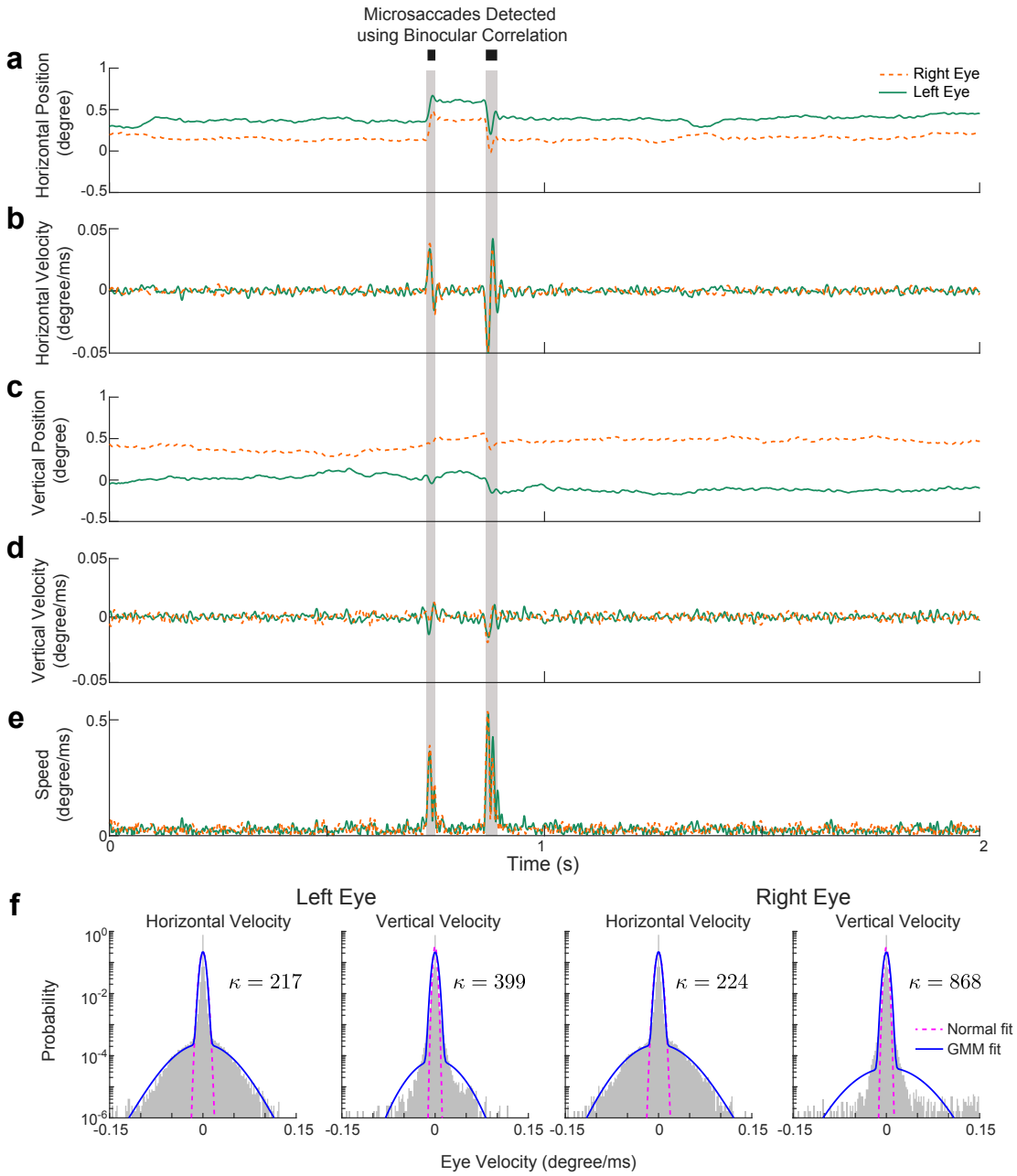

Extended Data Fig. 7. Reanalysis of the gaze fixation in humans, *Homo sapiens*.[21] (a–e) Representative temporal traces of horizontal eye position (a) and velocity (b), vertical eye position (c) and velocity (d), and eye speed (e) of right (orange dashed) and left (green) eye. The gray sections denote the detected microsaccades using the binoculer correlation (BC) method proposed in.[21] (f) Velocity histograms of horizontal and vertical velocities of left and right eye with respective kurtosis (κ) values. The magenta dashed and the blue solid curves correspond to a normal and GMM fit with three components, respectively. The dataset was collected from five human adults at 1000 Hz.

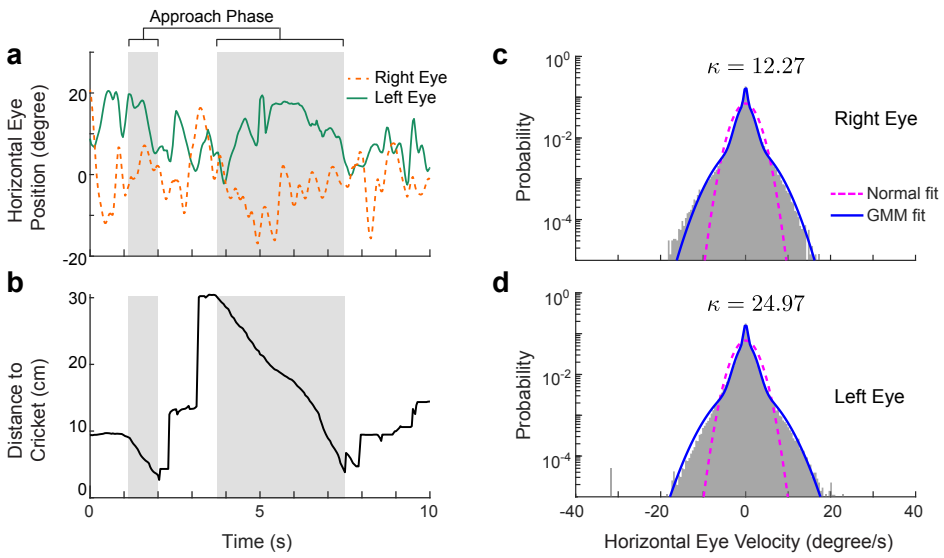

Extended Data Fig. 8. Reanalysis of the bilateral eye movements in house mice, *Mus musculus* during prey capture.[15] (a) Representative temporal traces of horizontal eye positions of right (orange dashed) and left (green) eye. (b) Representative plot of distance between the mouse and the cricket over time. The grey boxes denote the approach phases during which the mouse head was oriented towards the cricket (the azimuthal angle was with in $\pm 45^o$) and was moving at a speed over 1 cm/s For the present study, we focused on the data during the non-approach phases ($\sim 95\%$ of the total data). (c,d) Histograms of horizontal eye velocities of right (c) and left (d) eye during the non-approach phases with respective kurtosis (κ) values. The magenta dashed and the blue solid curves correspond to a normal and GMM fit with three components, respectively. The dataset has 105 trajectories, collected from seven mice at 30 Hz.

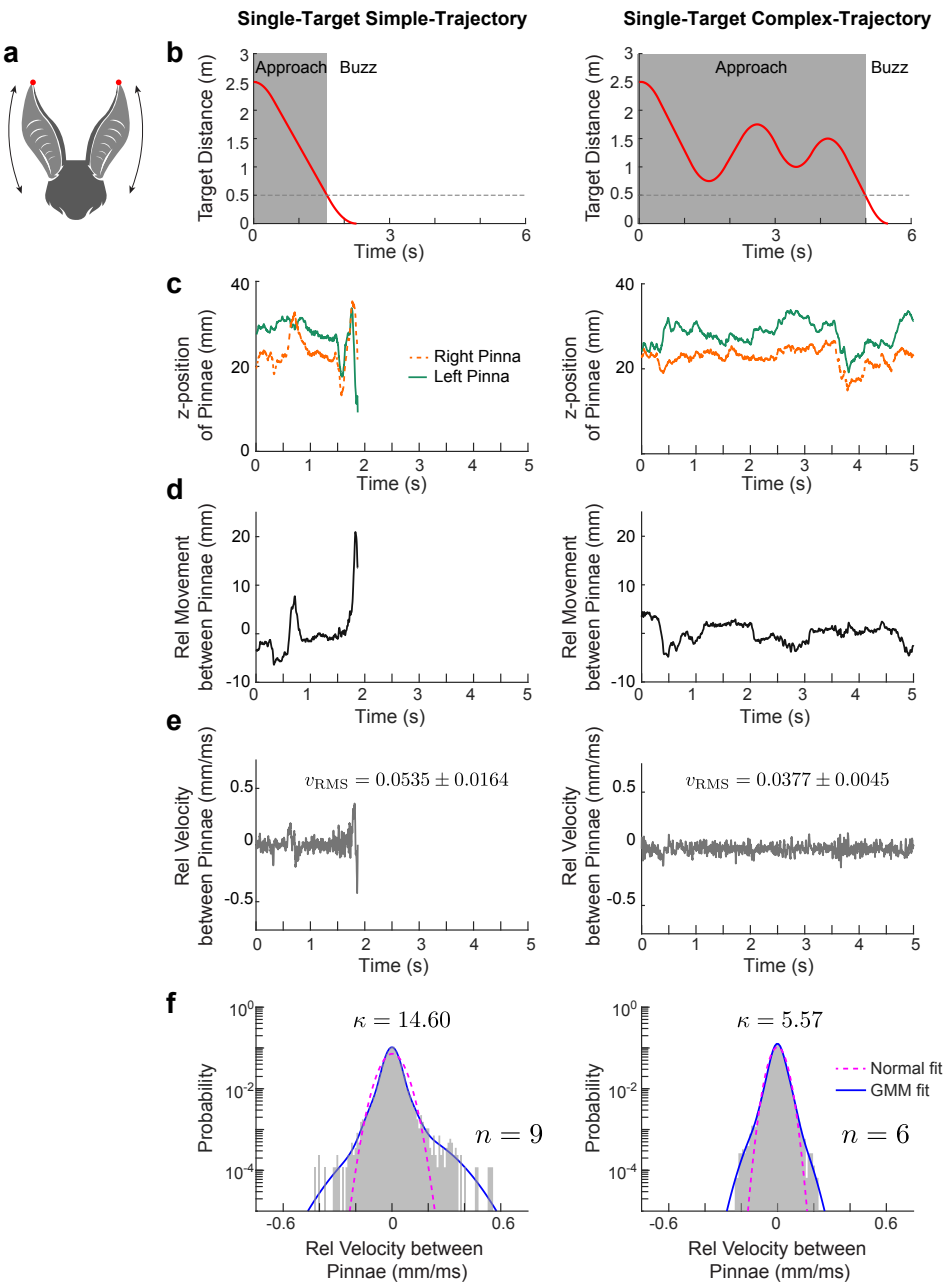

Extended Data Fig. 9. Reanalysis of the tip of the pinnae movement in big brown bats, *Eptesicus fuscus*.[16] (a) Cartoon showing the "head-waggle" behavior where bat changes the relative z-positions of the tip of its pinnae (red dots). (b) The simple (left) and the complex trajectory (right) of the tethered target (mealworm) over time. The gray box denotes the "approach" phase during which the target distance was greater than 0.5 m (dashed line). The rest we considered as the "buzz" phase. A sharp drop in the pulse duration and the pulse interval marked the beginning of the buzz phase and we found that the distance threshold 0.5 m roughly correlates to the onset of the buzz phase. For the present study, we focused on the data during the approach phase only (ignoring the last 200 frames). (c-f) Representative temporal traces of change in the z-positions (c) of the tip of the pinnae (orange dashed: right pinna, green: left pinna), relative movement (difference in z-positions) between pinnae (d), relative velocity between pinnae (e), and the histograms of relative velocity (f) with respective kurtosis (κ) values and the total number of trials (n) analyzed for the cases of the simple (left) and the complex trajectories (right). Mean $\pm$ SD of the RMS values of the relative velocity (v_{RMS}) are shown next to plots in (e). The one-tailed p-value $= 0.004$ for v_{RMS}, was computed using the Mann-Whitney-Wilcoxon test. The magenta dashed and the blue solid curves in (f) correspond to a normal and GMM fit with three components, respectively. The dataset has trajectories collected from three bats at 500 Hz.

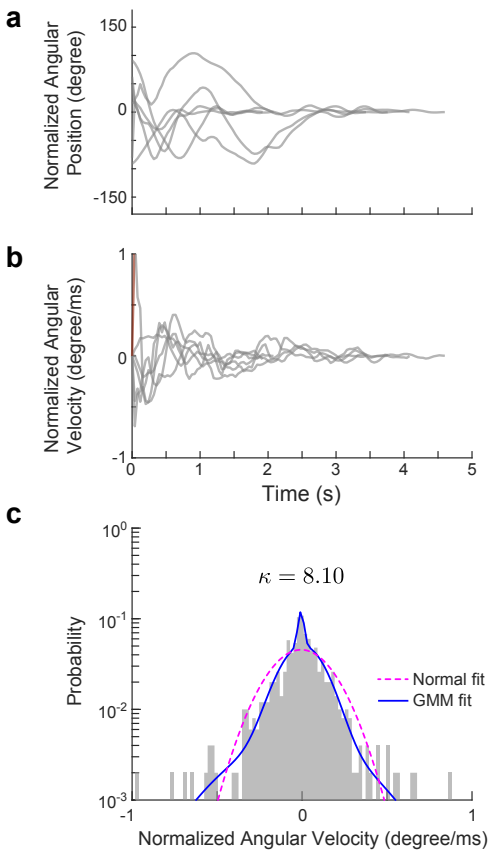

Extended Data Fig. 10. Reanalysis of the olfactory response in Eastern moles, *Scalopus aquaticus*.[14] (a) Temporal traces ($n = 6$) of angular position of moles normalized such that the destination direction was 0°. (b) Traces of angular velocity (assuming the data was sampled at 25 Hz). (c) Histograms of angular velocities with the kurtosis (κ) value. The magenta dashed and the blue solid curves correspond to a normal and GMM fit with three components, respectively.

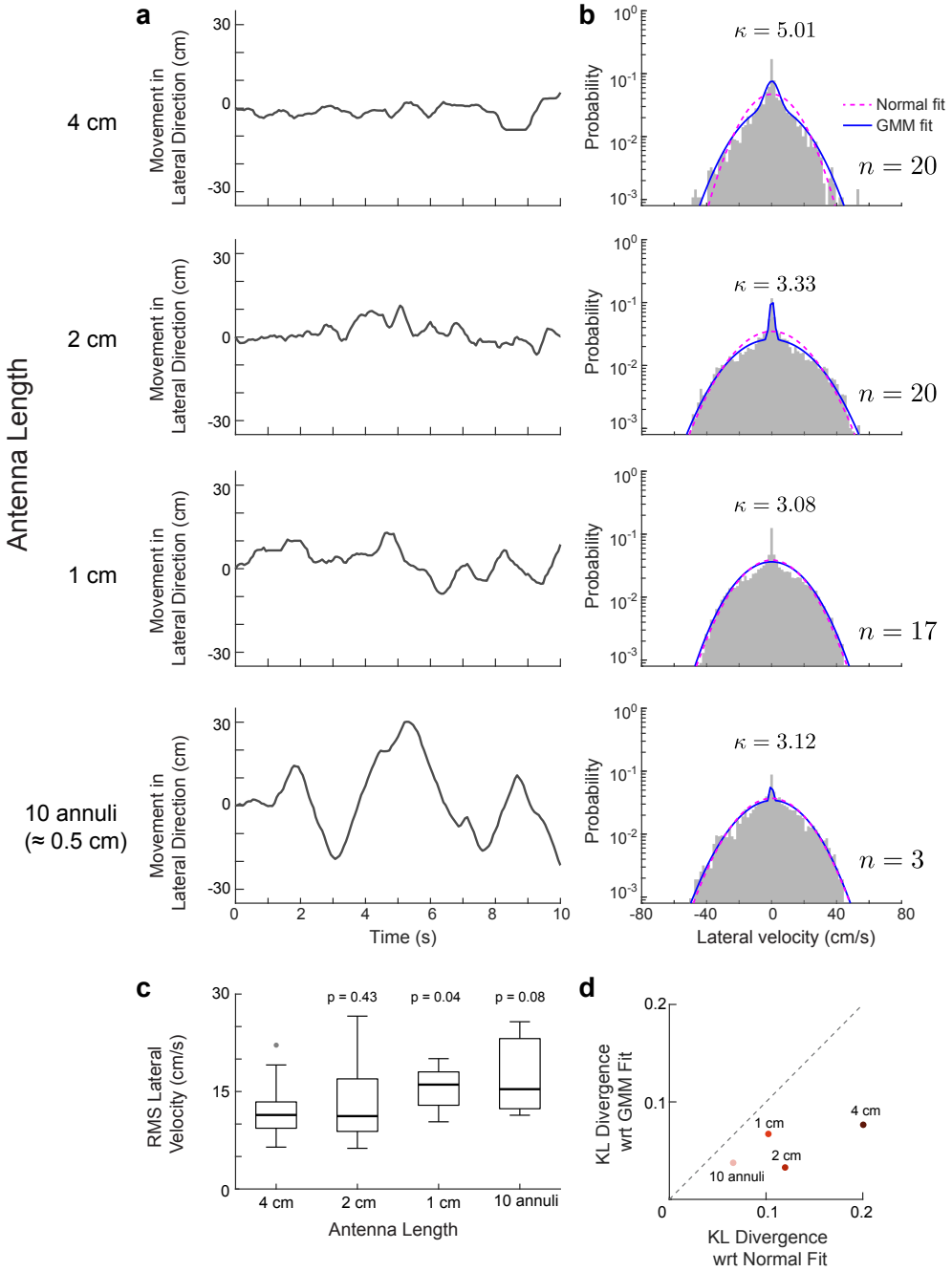

Extended Data Fig. 11. Reanalysis of the odor plume tracking response of American cockroach, *Periplaneta americana*.[18] (a,b) Representative temporal traces of the lateral head movement (a) and the histograms of the lateral velocities (b) for different antennae length as indicated. The magenta dashed and the blue solid curves in (b) correspond to a normal and GMM fit with three components, respectively. The dataset analyzed here, was collected at 30 Hz but later was subsampled at 15 Hz by the original study authors. The kurtosis (κ) values and the total number of trajectories (n) analyzed are indicated next to the respective panels in (b). (c) Comparison of the RMS lateral velocities for different experimental conditions. The one-tailed p-values were computed using the Mann-Whitney-Wilcoxon test with respect to the control case: 4 cm (intact antennae). (d) Plot of K-L divergence values for GMM fit vs Normal fit. Colors denote different experimental conditions. All the markers lying below the unity slope line indicated that the GMM better approximated the data.

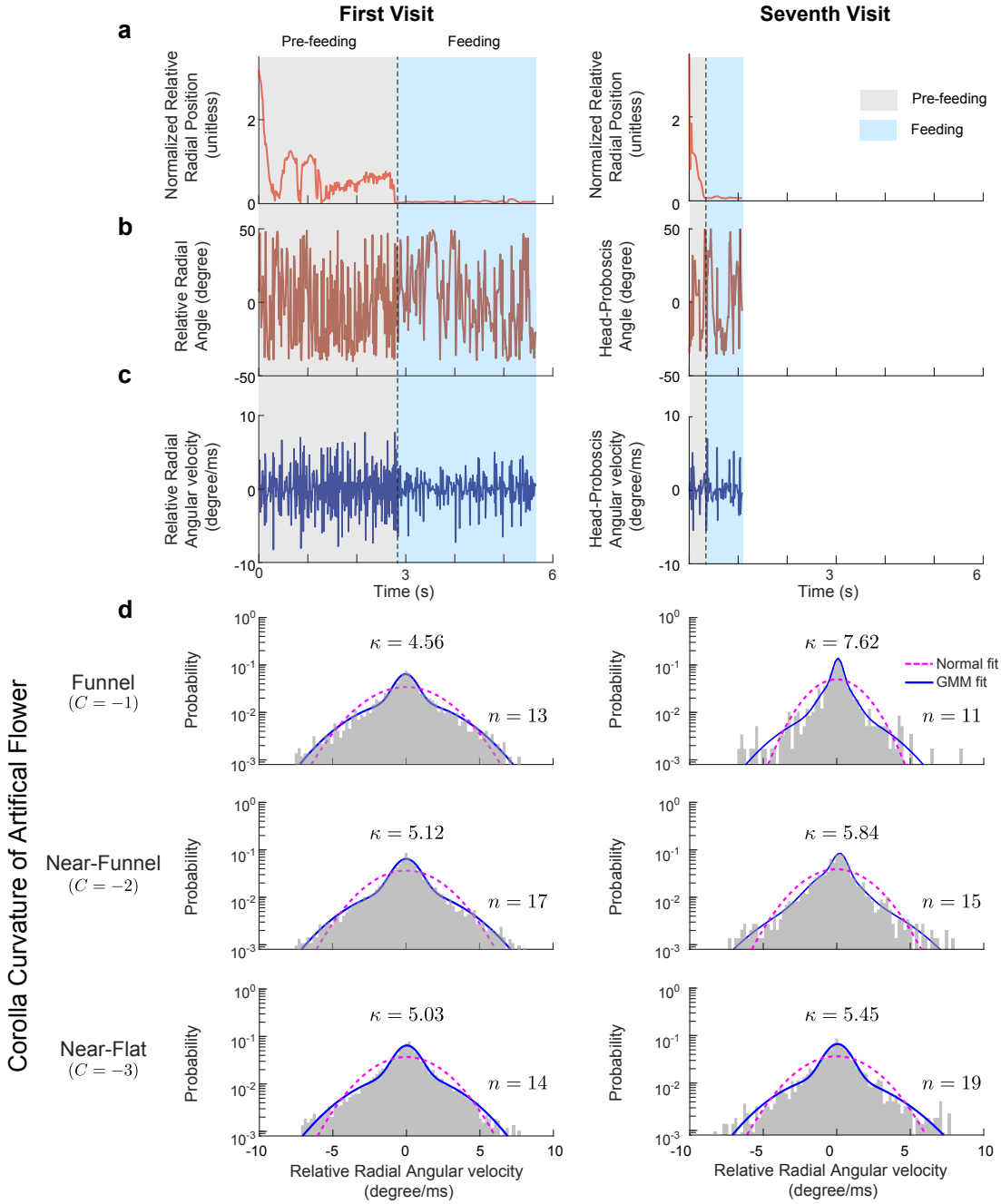

Extended Data Fig. 12. Reanalysis of the tactile response in crepuscular hawkmoth, *Manduca sexta*.[20] (a-c) Representative temporal traces of the normalized relative radial position (a), the relative radial orientation angle (b), and the relative radial angular velocity (c) during the first visit (left) and the seventh visit (early-learning; right) of the "funnel" type artificial flower by the hawkmoth. The gray and light blue boxes denote the pre-feeding and feeding phases, respectively. The dataset analyzed here was collected at 100 Hz. For the present study, we focused on the data during the pre-feeding phases only. (d) Histograms of relative radial angular velocity for different shape of the flower as indicated. "C" is the curvature parameter for the description of the lateral traces of the corollas. The magenta dashed and the blue solid curves in (d) correspond to a normal and GMM fit with three components, respectively. The kurtosis (κ) values and the total number of trajectories (n) analyzed are indicated next to the respective panels in (d).

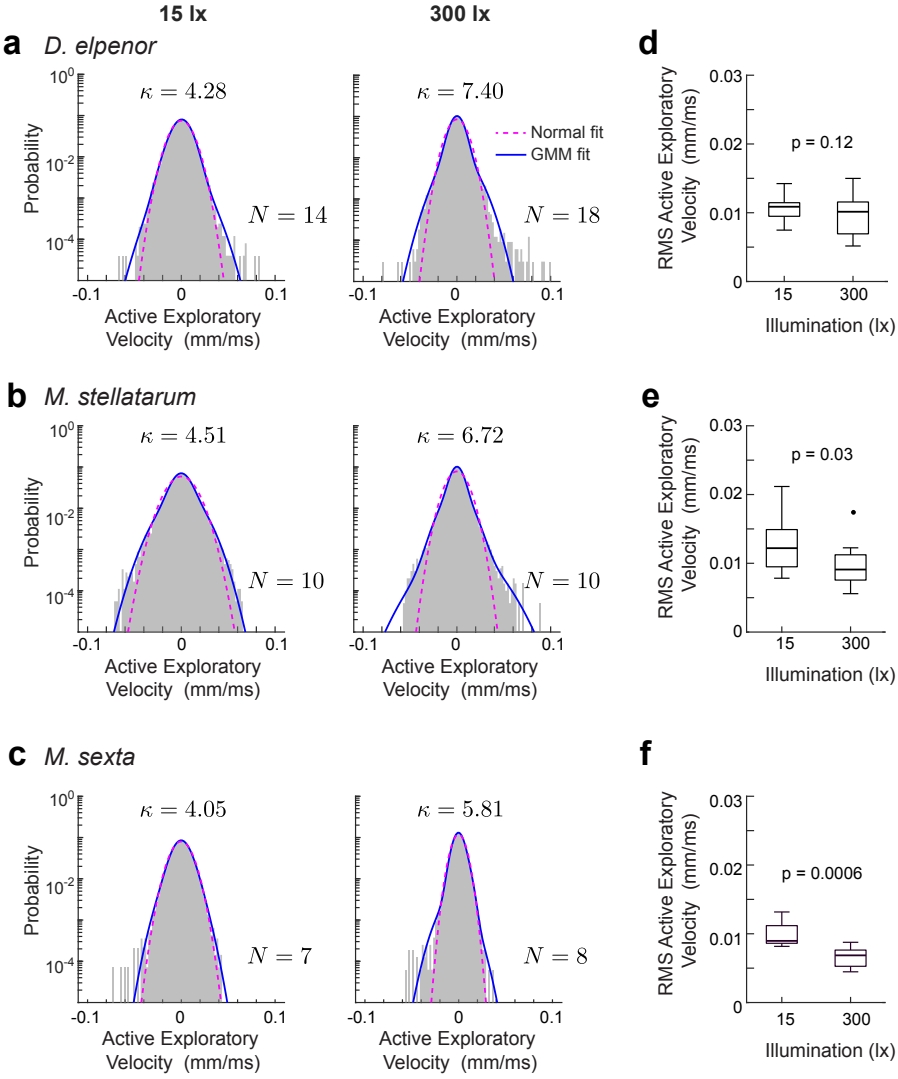

Extended Data Fig. 13. Reanalysis of the active exploratory movement of three different species of hawkmoths during flower tracking.[19] (a-c) Histograms of active exploratory velocity at low (left: 15 lx) and high (high: 300 lx) illumination level in three different species of hawkmoth—nocturnal *Deilephila elpenor* (A), diurnal *Macroglossum stellatarum* (b), and crepuscular *Manduca sexta* (c). The magenta dashed and the blue solid curves correspond to a normal and GMM fit with three components, respectively. The kurtosis (κ) values and the total number of hawkmoths (N) analyzed are indicated. (d-f) Box and whisker plots showing the RMS active exploratory velocity for all hawkmoths analyzed at different illumination levels. The one-tailed p-values were computed using the Mann-Whitney-Wilcoxon test. The datasets analyzed here were collected at 100 Hz with one trial per moth ($N = n$).

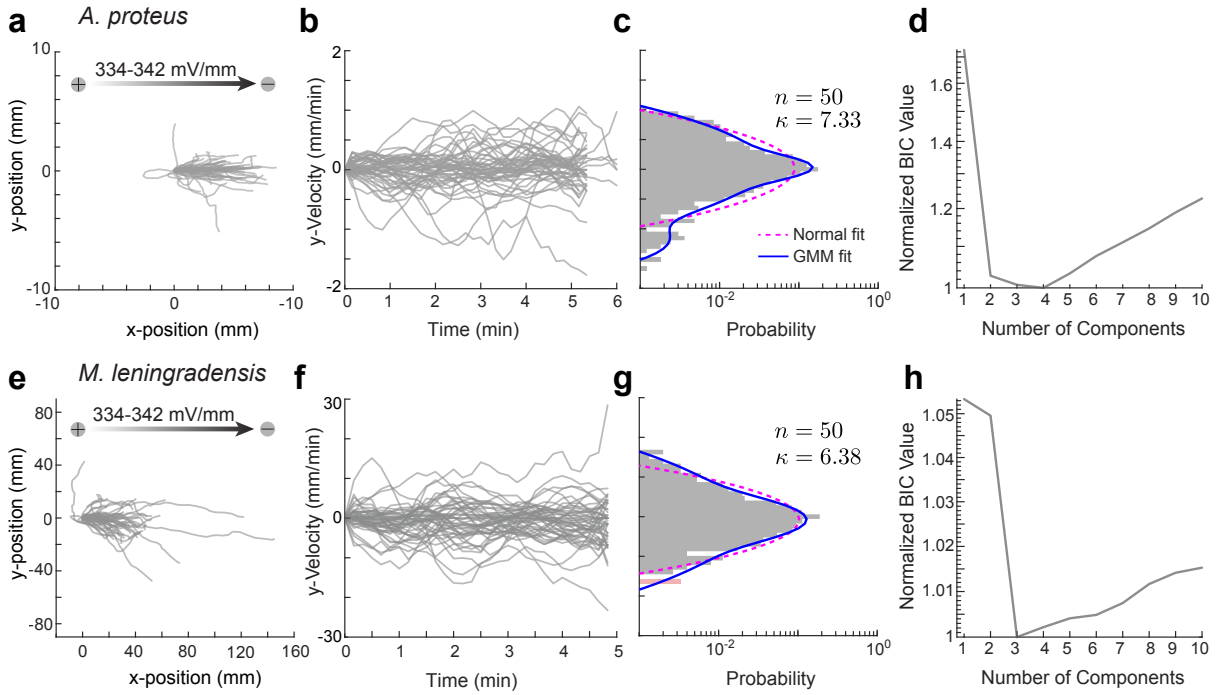

Extended Data Fig. 14. Reanalysis of the directed movement of *Amoeba proteus* and *Metamoeba leningradensis* in response to an electric field (galvaontaxis).[22] Migration trajectories ($n = 50$) of *A. proteus* (a), temporal traces of velocities (b) in the transverse direction of the applied electric field derived from the migration data, and the corresponding velocity histogram (c) with kurtosis (κ) value. The magenta dashed and the blue solid curves in (c) correspond to a normal and GMM fit with three components, respectively. (d) Plot of normalized Bayesian information criterion (BIC) value for varying number of components in the GMM model computed as a ratio with respect to the minimum BIC value obtained. (e-h) Galvanotaxis response in *M. leningradensis*. The panels are same as in (a-d). Image data for both datasets were collected at 0.1 Hz.

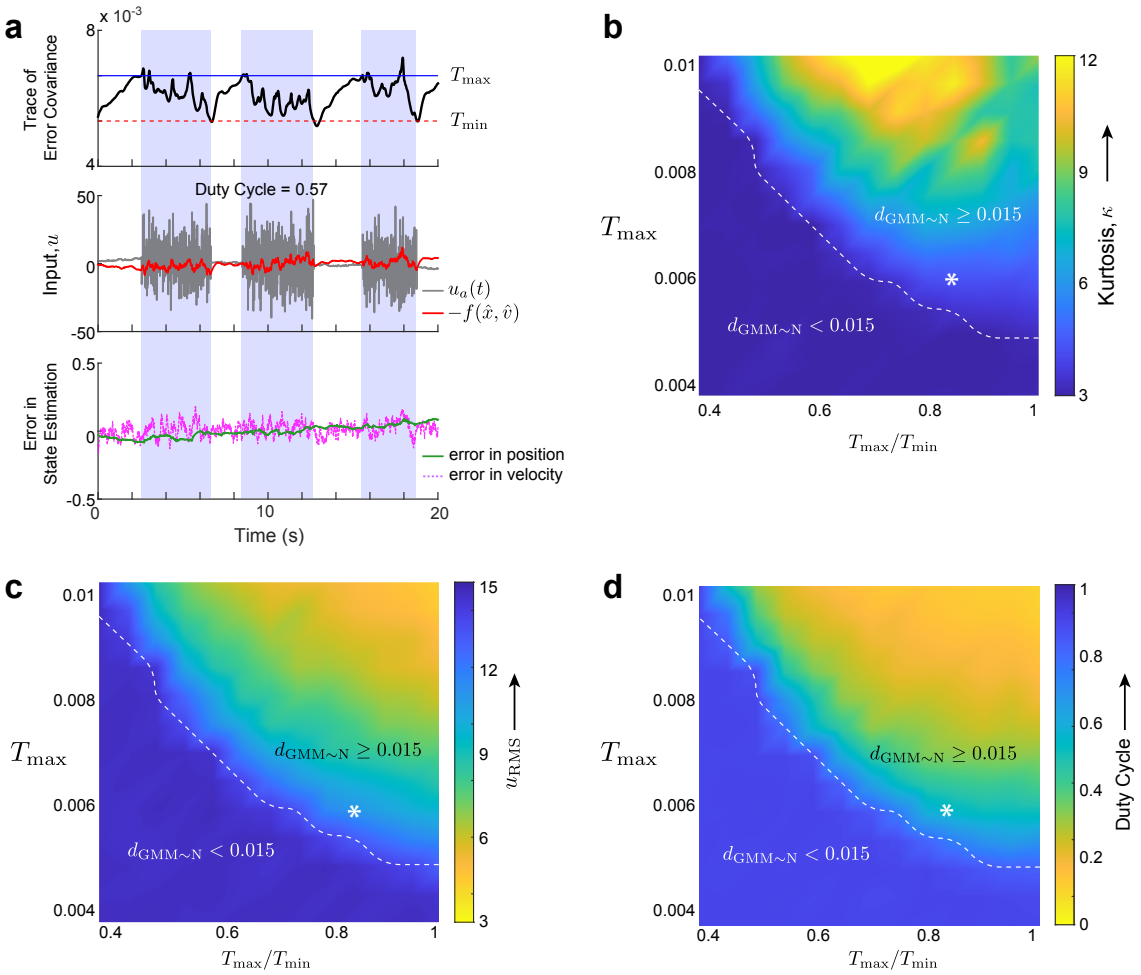

Extended Data Fig. 15. Triggered Excitation scheme and the effect of excitation thresholds, $T_{\min}$ and $T_{\max}$. (a) Temporal traces of the trace of the error covariance (M_ε) with threshold levels $T_{\min} = 0.005$ and $T_{\max} = 0.006$ (top), input u (middle; active control component, $u_a(t)$: gray; state-feedback component, $-f(\hat{x},\hat{v})$: red), and the state estimation errors (bottom) in position (green solid) and velocity (magenta dashed). The light blue boxes indicate the triggering instants. The triggering started as the trace of the error covariance exceeded $T_{\max}$ and the triggering continued till the trace of the error covariance dropped below $T_{\min}$. (b–d) Heatmaps showing kurtosis, κ (b) of the velocity distributions, RMS input energy, u_{RMS} (c), and the duty cycle of the input signal as thresholds $T_{\min}$ and $T_{\max}$ were varied. $T_{\max}$ was varied linearly from 0.004 to 0.01 where $T_{\min}$ was varied as the fraction of $T_{\max}$ from 0.4 to 1. From the left to right the relative difference between the thresholds decreased and finally merged to single threshold ($T_{\min} = T_{\max}$) at the end. The white dashed line in (b–d) shows the phase transition based on the absolute difference in the K-L divergences of normal and GMM fit to velocity distributions ($d_{GMM\sim N} = |D_{KL}(V||F_N) - D_{KL}(V||F_{GMM})|$). The region below the line corresponds to $d_{GMM\sim N} < 0.015$ and the region above corresponds to $d_{GMM\sim N} \geq 0.015$. Hence, the region above the line indicates the threshold pairs resulting velocity distributions were better fitted by GMM models. The asterisks denote the threshold values ($T_{\min} = 0.005, T_{\max} = 0.006$) used in (a).

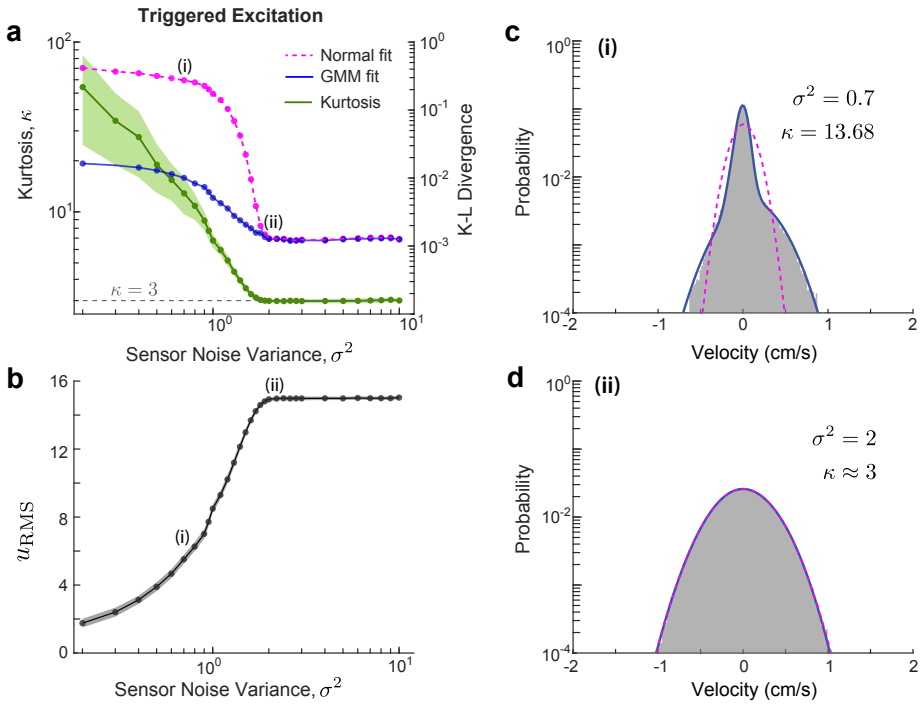

Extended Data Fig. 16. Velocity distribution tends toward a single-component Gaussian with increasing sensor noise in the model. (a) Variation of kurtosis, κ (green, left y-axis), and Kullback–Leibler (K-L) divergence (right y-axis) of normal distribution (magenta dashed) and Gaussian mixture model (blue solid) fit to the velocity distribution with sensor noise variance, σ^2. (b) Variation of RMS input with sensor noise variance, σ^2. The shaded regions in (a,b) denote the respective standard deviations ($n = 25$ independent simulations per σ^2). (c,d) Velocity histograms with kurtosis values are shown for sensor noise variance, $\sigma^2 = 0.70$ and 2, respectively, as indicated by (i) and (ii) in (a,b).

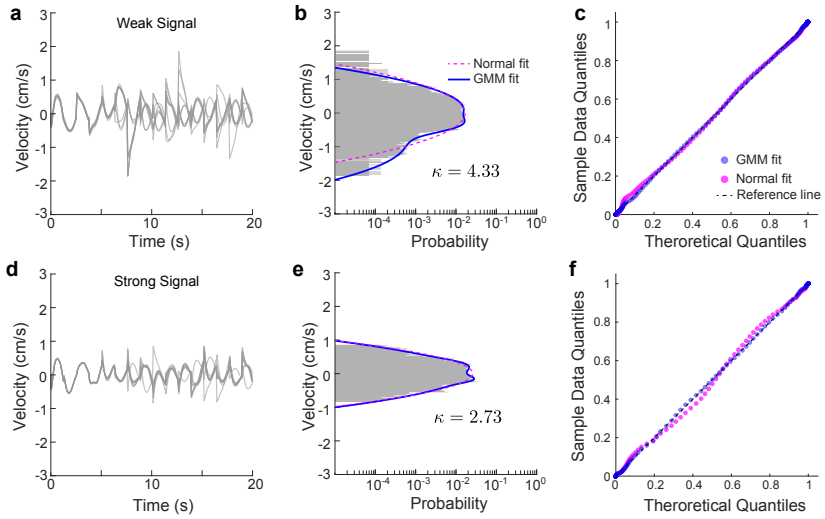

Extended Data Fig. 17. Reanalysis of the simulated trajectories for *Eigenmannia virescens* using Ergodic Harvesting Information (EIH) algorithm.[3] (a,b) Velocity traces ($n = 9$) for weak signal (a; SNR ≤ 30 dB equivalent to jamming amplitude ≥ 10 mA) and the corresponding histogram (b) with the kurtosis (κ) value. The magenta dashed and the blue solid curves correspond to a normal and Gaussian mixture model (GMM) fit with three components, respectively. (c) Q-Q plots comparing the sample velocity data for all trials ($n = 9$) from (a) with theoretical quantiles from the same normal (magenta) and GMM fit (blue) from (b). The fitting performances of GMM and the normal distribution were comparable. See Extended Data Table 4 for statistical details. (d–f) Velocity traces ($n = 9$) for strong signal (d; SNR ≥ 50 dB), corresponding histogram (e) with the kurtosis value, and the Q-Q plots (f). Colors and styles are same as in (a–c). Mean $\pm$ SD of the respective RMS values of the velocity (v_{RMS}) are shown on the panels (a,d).

Extended Data Tables

Extended Data Table 1: Comparison of Kullback-Leibler (K-L) divergence and Bayesian information criterion (BIC) for the three-component Gaussian mixture model (GMM) and normal fits to the velocity data of *Eigenmannia virescens* during lights-off and lights-on trials. GMM with lower values of K-L divergence and BIC is favored over normal.

			Fish Index				
			1	2	3	4	5
Lights off	GMM	K-L Divergence	0.026	0.017	0.013	0.021	0.027
		BIC ($\times 10^4$)	7.255	16.61	14.07	10.36	8.761
	Normal	K-L Divergence	0.346	0.107	0.075	0.261	0.162
		BIC ($\times 10^4$)	9.064	17.50	14.57	12.30	9.641
Lights on	GMM	K-L Divergence	0.049	0.058	0.024	0.055	0.051
		BIC ($\times 10^4$)	-3.573	-9.482	8.428	-3.780	-8.373
	Normal	K-L Divergence	0.949	0.268	0.315	0.991	0.363
		BIC ($\times 10^4$)	3.943	-7.464	10.80	4.163	-5.506

Extended Data Table 2: Summary of the reanalysis of the published data across nine different species[3,14–21] showing Kullback–Leibler (K-L) divergence and Bayesian information criterion (BIC) for the normal and the three-component Gaussian mixture model (GMM) fits to the velocity data and the kurtosis value (κ).

				K-L Divergence		BIC ($\times 10^4$)		
Species	Processes	Variables	Cases	GMM	Normal	GMM	Normal	κ
Human *Homo sapiens*	postural sway[17]	$v_{\text{ML CoM}}$	vision & touch	0.1161	0.2110	1.8477	2.3284	11.05
			vision	0.0596	0.1092	4.1721	4.4287	6.73
			touch	0.0358	0.0767	4.2073	4.4115	5.55
Human *Homo sapiens*	saccadic eye movement[21]	$v_{L,x}$		1.9921	2.3499	−2782	−2674	216.78
		$v_{R,x}$		1.9937	2.3720	−2782	−2669	223.98
		$v_{L,y}$		1.9826	1.8007	−2782	−2760	398.70
		$v_{R,y}$		1.9825	1.8223	−2783	−2746	868.06
House mice *Mus musculus*	bilateral eye movement[15]	$v_{L,x}$	non-approach	0.0230	0.2215	1.4644	1.6259	24.97
		$v_{R,x}$		0.0226	0.2204	1.4464	1.6020	12.27
Big brown bat *Eptesicus fuscus*	pinnae movement[16]	$\frac{dz_{L-R}}{dt}$	S-T S-T	0.0137	0.1639	−2.7253	−2.4706	14.60
			S-T C-T	0.0119	0.0483	−5.7678	−5.6557	5.57
Eastern mole *Scalopus aquaticus*	head movement[14]	ω_H	open nostrils	0.0902	0.2464	0.6482	0.6607	8.10
Glass knifefish *Eigenmannia virescens*	active exploration[3 a]	v_x	jamming off	0.0294	0.5031	−1.3302	0.4103	17.56
			jamming on	0.0166	0.0598	4.0278	4.1790	3.95
American cockroach *Periplaneta americana*	odor plume tracking[18]	$v_{H,y}$	4 cm[b]	0.0757	0.1997	2.1332	2.2367	5.01
			2 cm	0.0318	0.1189	7.5817	7.7385	3.33
			1 cm	0.0662	0.1016	8.2757	8.4790	3.08
			10 annuli	0.0366	0.0652	2.6725	2.6903	3.12
Carolina sphinx hawkmoth *Manduca sexta*	tactile sensing[20]	ω_{RRA}	1st visit: $C = -1$[c]	0.0190	0.1142	9.2494	9.3431	4.56
			1st visit: $C = -2$	0.0154	0.1243	14.992	15.170	5.12
			1st visit: $C = -3$	0.0158	0.1138	10.676	10.790	5.03
			7st visit: $C = -1$	0.0750	0.3288	1.0008	1.0283	7.62
			7st visit: $C = -2$	0.0316	0.1807	2.5886	2.6283	5.84
			7st visit: $C = -3$					5.45
Elephant hawkmoth *Deilephila elpenor*	Active exploration[19 d]	v_x	15 lux	0.0071	0.0167	30.43	30.47	4.28
			300 lux	0.0120	0.0549	39.05	39.34	7.40
Hummingbird hawkmoth *Macroglossum stellatarum*			15 lux	0.0054	0.0296	22.73	22.81	4.51
			300 lux	0.0088	0.0682	23.97	24.21	6.72
Carolina sphinx hawkmoth *Manduca sexta*			15 lux	0.01	0.0162	16.86	16.87	4.05
			300 lux	0.0162	0.0385	17.95	18.01	5.81

[a] From the refuge tracking response, the active exploration component is extracted following the method (eliminating frequency peak corresponding to the refuge motion) explained in Supplementary Material and Methods.
[b] intact antennae.
[c] $C = -1$: funnel, $C = -2$: near-funnel, $C = -3$: near flat.
[d] From the visual tracking response to swaying flower, the active exploration component is extracted following the method (eliminating frequency peaks corresponding to the flower motion) explained in Supplementary Material and Methods.

Notations used: $v_{\text{ML CoM}}$ = velocity of mediolateral center of mass, $v_{L,x}$ = horizontal velocity of left eye, $v_{R,x}$ = horizontal velocity of right eye, $v_{L,y}$ = vertical velocity of left eye, $v_{R,y}$ = vertical velocity of right eye, dz_{L-R}/dt: rate of change of difference in the z-positions of left and right pinna tips, S-T S-T: single-target simple-trajectory, S-T C-T: single-target complex-trajectory, ω_H: angular velocity of head, v_x: horizontal/longitudinal velocity, $v_{H,y}$ = lateral head velocity, ω_{RRA} = relative radial angular velocity,
The trend with Akaike information criterion (AIC) values (not shown) was similar to that of BIC.

Extended Data Table 3: Summary of comparison between different strategies of template model and Ergodic Information Harvesting (EIH) model showing Kullback-Leibler (K-L) divergence and Bayesian information criterion (BIC) for the normal and the three-component Gaussian mixture model (GMM) fits to the simulated velocity data and the kurtosis value (κ).

			K-L Divergence		BIC ($\times 10^4$)				
Models	Strategies	Sensory Noise	GMM	Normal	GMM	Normal	κ	$\Delta\kappa$	Comments
Template model	Zero Excitation		0.0076	0.0122	-1.7621	-1.7602	3.49	$\longleftrightarrow$	$\kappa \approx 3$ (constant) for low and high noise
	Persistent Excitation		0.0240	0.0240	0.7730	0.7688	2.94		
	Triggered Excitation	low ($\sigma^2 = 0.5$)	0.0129	0.3063	-2.0478	-1.3962	19.03	$\uparrow$	κ increases for low noise
		high ($\sigma^2 = 2$)	0.0015	0.0016	0.4569	0.4520	2.93		
EIH[3a]		low (SNR $>$ 50 dB)	0.0259	0.0508	-0.0088	0.0587	2.73	$\downarrow$	κ decreases for low noise[b]
		high (SNR $\leq$ 30 dB)	0.0170	0.0523	1.2027	1.2982	4.33		

[a]We used the same set of parameters specified in Chen *et al.*[3] From the simulated refuge tracking response, the active exploration component is extracted by eliminating the frequency peak corresponding to the refuge motion, as explained in Supplementary Material and Methods.

[b]EIH algorithm produces the trend of increasing kurtosis (κ) of velocity distributions for lower sensory salience opposite to what is observed in wide range of organisms i.e., decrease in kurtosis for lower sensory salience.[14–20, 22]

References

[1] Gibson, J. J. Observations on active touch. *Psychol Rev* **69**, 477–491 (1962).

[2] Biswas, D. *et al.* Closed-loop control of active sensing movements regulates sensory slip. *Curr Biol* **28**, 4029–4036 (2018).

[3] Chen, C., Murphey, T. D. & MacIver, M. A. Tuning movement for sensing in an uncertain world. *eLife* **9**, e52371 (2020).

[4] Soatto, S. Actionable information in vision. In *Machine learning for computer vision*, 17–48 (Springer, 2013).

[5] Golovin, D. & Krause, A. Adaptive submodularity: Theory and applications in active learning and stochastic optimization. *J Artif Intell Res* **42**, 427–486 (2011).

[6] Cooper, G. F. The computational complexity of probabilistic inference using Bayesian belief networks. *Artif Intell* **42**, 393–405 (1990).

[7] Blondel, V. D. & Tsitsiklis, J. N. A survey of computational complexity results in systems and control. *Automatica* **36**, 1249–1274 (2000).

[8] Yang, S. C.-H., Wolpert, D. M. & Lengyel, M. Theoretical perspectives on active sensing. *Curr Opin Behav Sci* **11**, 100–108 (2016).

[9] Stamper, S. A., Roth, E., Cowan, N. J. & Fortune, E. S. Active sensing via movement shapes spatiotemporal patterns of sensory feedback. *J Exp Biol* **215**, 1567–1574 (2012).

[10] Cowan, N. J. & Fortune, E. S. The critical role of locomotion mechanics in decoding sensory systems. *J Neurosci* **27**, 1123–1128 (2007).

[11] Roth, E., Zhuang, K., Stamper, S. A., Fortune, E. S. & Cowan, N. J. Stimulus predictability mediates a switch in locomotor smooth pursuit performance for *Eigenmannia virescens*. *J Exp Biol* **214**, 1170–1180 (2011).

[12] Sutton, E. E., Demir, A., Stamper, S. A., Fortune, E. S. & Cowan, N. J. Dynamic modulation of visual and electrosensory gains for locomotor control. *J. R. Soc. Interface* **13**, 20160057 (2016).

[13] Rose, G. J. & Canfield, J. G. Longitudinal tracking responses of the weakly electric fish, *Sternopygus*. *J Comp Physiol A* **171**, 791–798 (1993).

[14] Catania, K. C. Stereo and serial sniffing guide navigation to an odour source in a mammal. *Nat Commun* **4**, 1–8 (2013).

[15] Michaiel, A. M., Abe, E. T. & Niell, C. M. Dynamics of gaze control during prey capture in freely moving mice. *eLife* **9**, e57458 (2020).

[16] Wohlgemuth, M. J., Kothari, N. B. & Moss, C. F. Action enhances acoustic cues for 3-D target localization by echolocating bats. *PLoS Biol* **14**, e1002544 (2016).

[17] Kiemel, T., Oie, K. S. & Jeka, J. J. Multisensory fusion and the stochastic structure of postural sway. *Biol Cybern* **87**, 262–277 (2002).

[18] Lockey, J. K. & Willis, M. A. One antenna, two antennae, big antennae, small: total antennae length, not bilateral symmetry, predicts odor-tracking performance in the American cockroach *Periplaneta americana*. *J Exp Biol* **218**, 2156–2165 (2015).

[19] Stöckl, A. L., Kihlström, K., Chandler, S. & Sponberg, S. Comparative system identification of flower tracking performance in three hawkmoth species reveals adaptations for dim light vision. *Philos Trans R Soc Lond B Biol Sci* **372**, 20160078 (2017).

[20] Deora, T., Ahmed, M. A., Daniel, T. L. & Brunton, B. W. Tactile active sensing in an insect plant pollinator. *J Exp Biol* **224**, jeb239442 (2021).

[21] Hauperich, A.-K., Young, L. K. & Smithson, H. E. What makes a microsaccade? A review of 70 years of research prompts a new detection method. *J Eye Mov Res* **12** (2019).

[22] De la Fuente, I. M. *et al.* Evidence of conditioned behavior in amoebae. *Nat Commun* **10**, 1–12 (2019).

[23] Uyanik, I., Stamper, S. A., Cowan, N. J. & Fortune, E. S. Sensory cues modulate smooth pursuit and active sensing movements. *Front Behav Neurosci* **13**, 59 (2019).

[24] Sefati, S. *et al.* Mutually opposing forces during locomotion can eliminate the tradeoff between maneuverability and stability. *Proc Natl Acad Sci U.S.A.* **110**, 18798–18803 (2013).

[25] Narendra, K. S. & Annaswamy, A. M. Persistent excitation in adaptive systems. *Int J Control* **45**, 127–160 (1987).

[26] Kunapareddy, A. & Cowan, N. J. Recovering observability via active sensing. In *Proc Amer Control Conf*, 2821–2826 (IEEE, Milwaukee, WI, USA, 2018).

[27] Sontag, E. D., Biswas, D. & Cowan, N. J. An observability result related to active sensing (2022). URL `https://arxiv.org/abs/2210.03848`.

[28] Fabre, M. *et al.* Large postural sways prevent foot tactile information from fading: Neurophysiological evidence. *Cereb Cortex Comm* **2** (2020).

[29] Arkley, K., Grant, R. A., Mitchinson, B. & Prescott, T. J. Strategy change in vibrissal active sensing during rat locomotion. *Curr Biol* **24**, 1507–1512 (2014).

[30] Nelson, M., Xu, Z. & Payne, J. Characterization and modeling of p-type electrosensory afferent responses to amplitude modulations in a wave-type electric fish. *J Comp Physiol A* **181**, 532–544 (1997).

[31] Lee, J. *et al.* Templates and anchors for antenna-based wall following in cockroaches and robots. *IEEE Trans Robot* **24**, 130–143 (2008).

[32] Jun, J. J., Longtin, A. & Maler, L. Active sensing associated with spatial learning reveals memory-based attention in an electric fish. *J Neurophysiol* **115**, 2577–2592 (2016).

[33] Mobbs, D., Trimmer, P. C., Blumstein, D. T. & Dayan, P. Foraging for foundations in decision neuroscience: insights from ethology. *Nat Rev Neurosci* **19**, 419–427 (2018).

[34] Kaelbling, L. P., Littman, M. L. & Moore, A. W. Reinforcement learning: A survey. *J Artif Intell Res* **4**, 237–285 (1996).

[35] Zweifel, N. O. & Hartmann, M. J. Defining "active sensing" through an analysis of sensing energetics: homeoactive and alloactive sensing. *J Neurophys* **124**, 40–48 (2020).

[36] Bullock, T. H. Electroreception. *Annu Rev Neurosci* **5**, 121–170 (1982).

[37] Brinkløv, S., Elemans, C. P. & Ratcliffe, J. M. Oilbirds produce echolocation signals beyond their best hearing range and adjust signal design to natural light conditions. *R Soc Open Sci* **4**, 170255 (2017).

[38] Nelson, M. E. & MacIver, M. A. Sensory acquisition in active sensing systems. *J Comp Physiol A* **192**, 573–586 (2006).

[39] Snyder, J. B., Nelson, M. E., Burdick, J. W. & MacIver, M. A. Omnidirectional sensory and motor volumes in electric fish. *PLoS Biol* **5**, e301 (2007).

[40] Ghose, K. & Moss, C. F. Steering by hearing: a bat's acoustic gaze is linked to its flight motor output by a delayed, adaptive linear law. *J Neurosci* **26**, 1704–1710 (2006).

[41] Berg, H. C. & Brown, D. A. Chemotaxis in *Escherichia coli* analysed by three-dimensional tracking. *Nature* **239**, 500–504 (1972).

[42] Benda, J., Longtin, A. & Maler, L. A synchronization-desynchronization code for natural communication signals. *Neuron* **52**, 347–358 (2006).

[43] Metzen, M. G., Hofmann, V. & Chacron, M. J. Neural synchrony gives rise to amplitude-and duration-invariant encoding consistent with perception of natural communication stimuli. *Front Neurosci* **14**, 79 (2020).

[44] Hofmann, V. & Chacron, M. J. Population coding and correlated variability in electrosensory pathways. *Front Integr Neurosci* **12**, 56 (2018).

[45] Grewe, J., Kruscha, A., Lindner, B. & Benda, J. Synchronous spikes are necessary but not sufficient for a synchrony code in populations of spiking neurons. *Proc Natl Acad Sci U.S.A.* **114**, E1977–E1985 (2017).

[46] Fetcho, J. R., Higashijima, S.-i. & McLean, D. L. Zebrafish and motor control over the last decade. *Brain Res Rev* **57**, 86–93 (2008).

[47] Tabor, K. M. *et al.* Direct activation of the Mauthner cell by electric field pulses drives ultrarapid escape responses. *J Neurophysiol* **112**, 834–844 (2014).

[48] Hitschfeld, É. M., Stamper, S. A., Vonderschen, K., Fortune, E. S. & Chacron, M. J. Effects of restraint and immobilization on electrosensory behaviors of weakly electric fish. *ILAR journal* **50**, 361–372 (2009).

[49] Vágvölgyi, B. P. General tracker. `https://github.com/vagvolgyi/general_tracker` (2021).

[50] Matthews, M. & Sponberg, S. Hawkmoth flight in the unsteady wakes of flowers. *J Exp Biol* **221**, jeb179259 (2018).

[51] Tritico, H. M. & Cotel, A. J. The effects of turbulent eddies on the stability and critical swimming speed of creek chub *Semotilus atromaculatus*. *J Exp Biol* **213**, 2284–2293 (2010).

[52] Harris, C. M. & Wolpert, D. M. Signal-dependent noise determines motor planning. *Nature* **394**, 780–784 (1998).

[53] Ratcliffe, J. M., Elemans, C. P., Jakobsen, L. & Surlykke, A. How the bat got its buzz. *Biol Lett* **9**, 20121031 (2013).